Brain, Behavior, and Immunity 106 (2022) 49–66

Contents lists available at ScienceDirect

Brain Behavior and Immunity

journal homepage: www.elsevier.com/locate/ybrbi

Full-length Article

Early posttraumatic CSF1R inhibition via PLX3397 leads to time- and sex-dependent effects on inflammation and neuronal maintenance after traumatic brain injury in mice

Yong Wang [a], Isa Wernersbach [a], Jenny Strehle [a], Shuailong Li [a], Dominik Appel [a], Matthias Klein [b], Katharina Ritter [a], Regina Hummel [a], Irmgard Tegeder [c], Michael K.E. Schäfer [a,d,e,*]

[a] Department of Anesthesiology, University Medical Center, Johannes Gutenberg-University Mainz, Langenbeckstr. 1, 55131 Mainz, Germany
[b] Institute for Immunology, University Medical Center, Johannes Gutenberg-University Mainz, Langenbeckstr. 1, 55131 Mainz, Germany
[c] Institute of Clinical Pharmacology, Goethe-University Frankfurt, Medical Faculty, Theodor Stern Kai 7, 60590 Frankfurt, Germany
[d] Focus Program Translational Neurosciences (FTN) of the Johannes Gutenberg-University Mainz, Langenbeckstr. 1, 55131 Mainz, Germany
[e] Research Center for Immunotherapy (FZI), Johannes Gutenberg-University Mainz, Langenbeckstr. 1, 55131 Mainz, Germany

ARTICLE INFO

Keywords:
Traumatic brain injury
Colony stimulating factor 1 receptor
Microglia
Inflammation
Phagocytosis
Hematoma
Therapy
RNAseq
Synapse
Sex

ABSTRACT

Background: There is a need for early therapeutic interventions after traumatic brain injury (TBI) to prevent neurodegeneration. Microglia/macrophage (M/M) depletion and repopulation after treatment with colony stimulating factor 1 receptor (CSF1R) inhibitors reduces neurodegeneration. The present study investigates short- and long-term consequences after CSF1R inhibition during the early phase after TBI.

Methods: Sex-matched mice were subjected to TBI and CSF1R inhibition by PLX3397 for 5 days and sacrificed at 5 or 30 days post injury (dpi). Neurological deficits were monitored and brain tissues were examined for histo- and molecular pathological markers. RNAseq was performed with 30 dpi TBI samples.

Results: At 5 dpi, CSF1R inhibition attenuated the TBI-induced perilesional M/M increase and associated gene expressions by up to 50%. M/M attenuation did not affect structural brain damage at this time-point, impaired hematoma clearance, and had no effect on IL-1β expression. At 30 dpi, following drug discontinuation at 5 dpi and M/M repopulation, CSF1R inhibition attenuated brain tissue loss regardless of sex, as well as hippocampal atrophy and thalamic neuronal loss in male mice. Selected gene markers of brain inflammation and apoptosis were reduced in males but increased in females after early CSF1R inhibition as compared to corresponding TBI vehicle groups. Neurological outcome in behaving mice was almost not affected. RNAseq and gene set enrichment analysis (GSEA) of injured brains at 30 dpi revealed more genes associated with dendritic spines and synapse function after early CSF1R inhibition as compared to vehicle, suggesting improved neuronal maintenance and recovery. In TBI vehicle mice, GSEA showed high oxidative phosphorylation, oxidoreductase activity and ribosomal biogenesis suggesting oxidative stress and increased abundance of metabolically highly active cells. More genes associated with immune processes and phagocytosis in PLX3397 treated females vs males, suggesting sex-specific differences in response to early CSF1R inhibition after TBI.

Conclusions: M/M attenuation after CSF1R inhibition via PLX3397 during the early phase of TBI reduces long-term brain tissue loss, improves neuronal maintenance and fosters synapse recovery. Overall effects were not sex-specific but there is evidence that male mice benefit more than female mice.

1. Introduction

Traumatic brain injury (TBI) is a major cause of death and disability and represents a severe medical and socioeconomic burden (Dewan et al., 2018). Age and sex have been associated with a negative outcome, complications and chronic symptoms after TBI (Hosomi et al., 2021).

* Corresponding author at: Department of Anesthesiology, University Medical Center, Johannes Gutenberg-University Mainz, Langenbeckstr. 1, 55131 Mainz, Germany.
E-mail address: michael.Schaefer@unimedizin-mainz.de (M.K.E. Schäfer).

https://doi.org/10.1016/j.bbi.2022.07.164
Received 25 April 2022; Received in revised form 8 July 2022; Accepted 30 July 2022
Available online 3 August 2022

Despite the identification of neuroprotective drugs in animal models of TBI and decades of clinical research, therapeutic options are limited to surgical interventions and symptomatic relief (McConeghy et al., 2012), owing to the complexity of pathophysiological processes comprising cerebral ischemia, impaired cerebral blood flow, blood brain barrier disruption, brain edema, oxidative stress, mitochondrial dysfunction, and neural cell death (Abdul-Muneer et al., 2015; Akamatsu and Hanafy, 2020; Schäfer et al., 2014; Werner and Engelhard, 2007). TBI pathology is associated with a clinically relevant neuroinflammation which develops early and persists for months to years after TBI (Morganti-Kossmann et al., 2019; Ramlackhansingh et al., 2011). Neuroinflammation is mediated by different types of brain resident cells, most notably microglia and astrocytes (Karve et al., 2016). Together with peripheral immune cells, that infiltrate the injured brain tissue, they generate a highly inflammatory environment at injury sites, which is detrimental for neuronal survival but necessary to facilitate tissue clearance, glial scar formation, and neural repair (Bolte and Lukens, 2021; Schäfer and Tegeder, 2018). Microglia/macrophages (M/M) play a central role during early and late phases of TBI mediating both beneficial and detrimental processes. These dual functions have been attributed to opposing polarization states, i.e. M1 and M2 (Donat et al., 2017; Loane and Kumar, 2016), but there is now consensus that microglia do not display distinct M1 or M2 phenotypes but rather display a mixed phenotype after brain injury (Jassam et al., 2017; Morganti-Kossmann et al., 2019; Ransohoff, 2016).

Microglia depletion strategies are considered promising translational therapies for neurological disorders including TBI (Green et al., 2020; Han et al., 2019). In particular, the small molecule inhibitors PLX3397 and PLX5622 that target the colony stimulating factor 1 receptor (CSF1R) that is pivotal for survival and proliferation of microglia, are able to deplete microglia in the brain (Elmore et al., 2014). Administration of CSF1R inhibitors prior to experimental TBI revealed important insights into the function of M/M during brain injury progression (Ritzel et al., 2021; Wang et al., 2020; Willis et al., 2020; Witcher et al., 2021; Witcher et al., 2018). In addition, M/M depletion in the subacute or in the chronic phase of TBI followed by microglia repopulation after discontinuation of the CSF1R inhibitor PLX5622 was shown to reduce neuropathology and neurological deficits in mice (Bray et al., 2022; Henry et al., 2020).

These and other studies identified small molecule inhibitors of CSF1R as powerful tools in brain injury research and highlighted the potential value of microglia depletion and repopulation in developing therapeutic approaches and proposed that repopulated microglia resolve ongoing neuroinflammation (Green et al., 2020; Han et al., 2019; Waisman et al., 2015). As mentioned, previous studies using CSF1R inhibitors in experimental TBI focused on pre-treatment strategies (Ritzel et al., 2021; Wang et al., 2020; Willis et al., 2020; Witcher et al., 2021; Witcher et al., 2018), or administration at subacute or chronic time-points (Bray et al., 2022; Henry et al., 2020). However, little is known about the consequences of post-traumatic administration of CSF1R inhibitor during the acute and early phases of TBI. Moreover, sex-specific effects, which are known to play a role in TBI as well as microglia functions (Caplan et al., 2017; Han et al., 2021; Newell et al., 2020; Villapol et al., 2017), have not yet been investigated in response to CSF1R inhibition after TBI.

In the current study, we addressed the existing need for early therapeutic interventions and tested the hypothesis that CSF1R inhibition during the early phase of TBI reduces pathological short- and long-term sequelae, also considering sex as a biological variable. Therefore, we subjected male and female C57Bl/6 mice to TBI using the controlled cortical impact (CCI) model and treated them for 5 days with the CSF1R inhibitor PLX3397 or vehicle. We investigated short- and long-term effects, using behavioral, histopathological, and molecular analyses including global transcriptomics.

2. Material and Methods

2.1. Animals and TBI experiments

Adult, 12–14 weeks-old, male and female C57BL6/J mice (Janvier Germany) were housed and maintained in a controlled environment (12 h dark/light cycle from 7:00 am to 19:00 pm, 22 ± 1 °C, 50 ± 5 % humidity) with food and water ad libitum. All experiments were performed according to the institutional guidelines of the Johannes Gutenberg University, Mainz, Germany, approved by the Animal Care and Ethics Committee of the Landesuntersuchungsamt Rheinland-Pfalz (protocol number G19-1–027), and in accordance with the ARRIVE guidelines. TBI/sham experiments were performed during daytime from 8:00 am to 18:00 pm in a randomized manner regarding TBI or sham surgery. Mice were treated essentially as described (Ritter et al., 2021), with carprofen for analgesia 30 min prior to anesthesia induced with 4 vol% isoflurane for 90 s and maintained with 2.1 vol% isoflurane for the whole procedure. After reaching satisfied depth of anesthesia, lidocaine was applied subcutaneously to the temples and the heads were immobilized in a stereotactic frame (Kopf Instruments). The temperature was maintained at 37 °C using feedback heating (Hugo Sachs, March-Hugstetten, Germany). A 1 cm skin incision was cut along the midline and a craniotomy of 4 × 4 mm was drilled above the right parietal cortex, and the displaced bone fragment was flapped laterally while keeping the dura mater intact. The cortical impact was applied using a Benchmark™ Stereotaxic Impactor (Leica Biosystems, Wetzlar, Germany): impactor tip diameter: 3 mm, velocity: 6 m/s, duration: 200 ms, displacement: 1.5 mm. After hemostasis, the displaced skull bone fragment was placed back to the burr hole and sealed with tissue glue, then the skin incision was sutured. Sham mice received isoflurane anesthesia, skin incision, and sutures, but no skull drilling, and impact. (Mice were placed in a temperature (36 °C) controlled incubator (IC8000, Draeger, Luebeck, Germany) after surgery, woke up within 10 min, and transferred back to the home cages after 90 min. Parameters including rectal temperature and duration of operation were recorded (Supplementary information, Table S1). All animals survived the CCI/sham procedure until the end of the observation periods.

2.2. Experimental design and pharmacological treatment

In total 80 mice were investigated in two independent cohorts with survival times of 5 days (cohort 1) or 30 days (cohort 2) after TBI, respectively (Fig. 1A, 6A, created with BioRender.com). In each cohort, mice were assigned randomly to four experimental groups with equal sex distribution (TBI + PLX3397, n = 12; TBI + vehicle, n = 12; sham + PLX3397, n = 8; sham + vehicle, n = 8). Chow was purchased from Research Diets and animals from both cohorts received ad libitum either PLX3397 (290 mg/kg) or vehicle chow starting 90 min after the CCI/sham procedure for 5 days. The efficiency of dietary PLX3397 administration in adult mice was shown before with a 50 % reduction after 3 days and an elimination after 21 days of treatment (Elmore et al., 2014). Mice from cohort 2 were returned to the vehicle chow diet until 30 dpi. Food intake was determined daily from 1 dpi to 5 dpi (Supplementary information, Fig. S1, Table S2) and body weight of mice was determined at 1 dpi, 3 dpi, and 5 dpi (Supplementary information, Fig. S2, Table S3). Mice were killed at 5 dpi (cohort 1) or 30 dpi (cohort 2). Two experimenters performed the animal experiments in each cohort, one for surgery and one for drug administration and behavior. The latter were blind to the surgical procedure and treatment, subsequent data collection and analyses.

2.3. Evaluation of neurological deficits (NSS) and behavioral monitoring

Behavioral monitoring to assess neurological deficits was carried out in the same order as the CCI/sham surgeries during daytime from 9:00 am to 15:00 pm by experimenters blind to experimental groups. NSS was

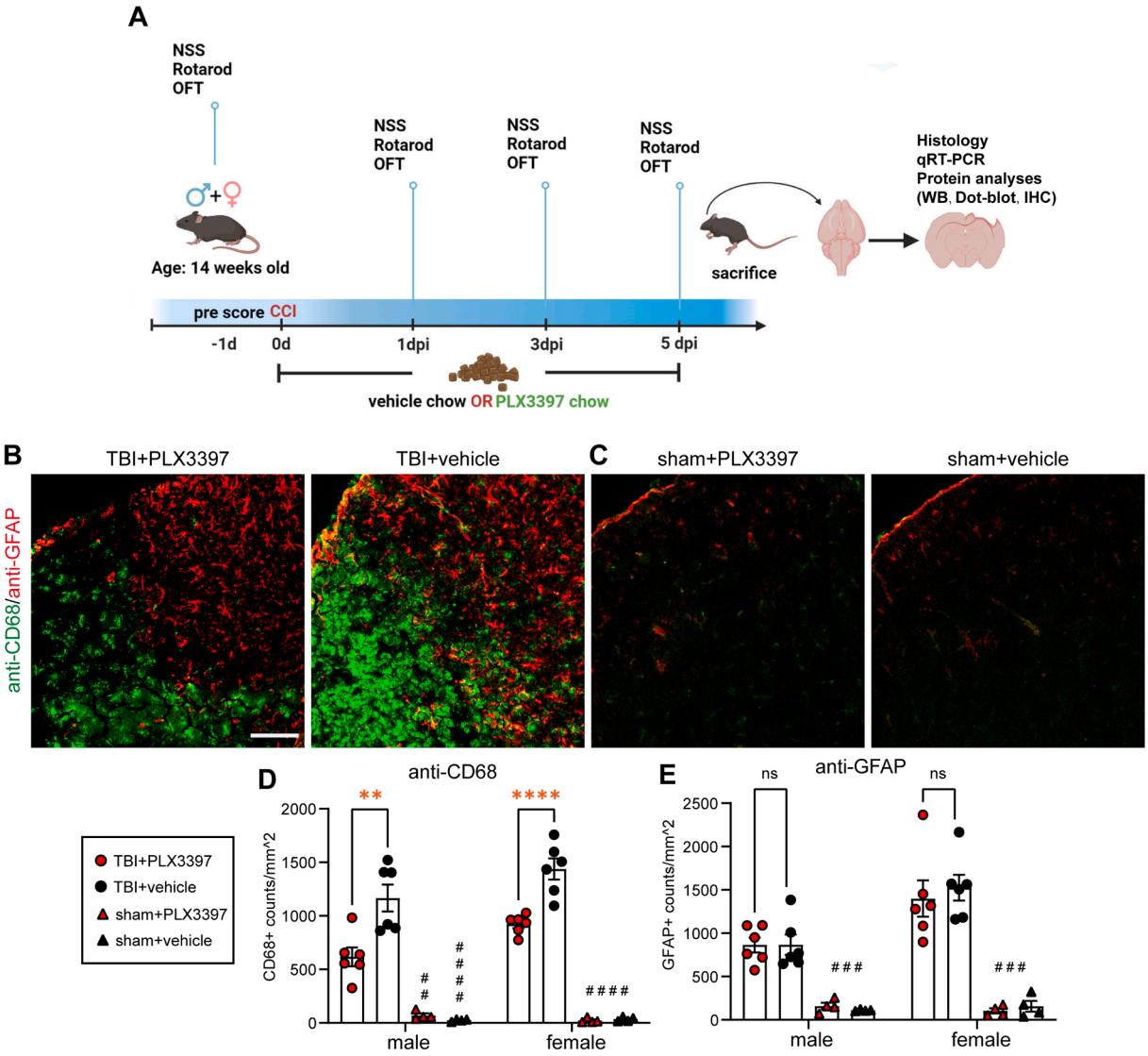

Fig. 1. CSF1R inhibition attenuates M/M accumulation in the early phase of TBI (A) Experimental design of 5 days survival groups (cohort 1, equal sex ratio). Neurological Severity Score (NSS), rotarod performance (RR) and open field test (OFT) were conducted at 1 day before TBI, at 1, 3 and 5 dpi. Animals received PLX3397 (290 mg/kg body weight) or vehicle chow for 5 days. At 5 dpi, brains were dissected and processed for histology, mRNA and protein analyses. (B) anti-CD68/anti-GFAP double-immunostaining showing that PLX3397 attenuated M/M accumulation but did not affect astrogliosis at 5 dpi. (C) Brains from sham mice treated with PLX3397 or vehicle did not show M/M accumulation or astrogliosis. (D, E) Counts of $CD68^+$ M/M and $GFAP^+$ astrocytes showing that CSF1R inhibition attenuated M/M accumulation regardless of sex TBI: n = 6, sham: n = 4, per group. Two-Way ANOVA followed by Holm Šídák s multiple comparisons test (D, E). Values from individual animals and mean ± SEM are shown. *indicates PLX3397 vs vehicle, ****$p < 0.0001$, $^{\#}$indicates TBI vs sham, $^{\#\#}p < 0.01$, $^{\#\#\#\#}p < 0.0001$, ns = not significant. Scale: 100 μm (B, C).

used to assess neurological deficits comprising balance, motor ability and general behavior one day before TBI and at different time points after TBI (Hummel et al., 2020). The minimum neurological score was 0 (no impairment) and the maximum was 12 (severe neurological dysfunction). Pre-scoring yielded almost zero scores, as expected. Sensorimotor coordination was tested by the Rotarod task (RR) as previously described (Hummel et al., 2020). Briefly, mice were tested on an accelerating RotaRod (Panlab RotaRod, Harvard Apparatus, Holliston, MA) and the latency to fall (height 18.5 cm) was recorded. The best value from two trials per animal and time point was analyzed. Animals completed four training trials one day before TBI, followed by two trials to determine the pre-injury rotarod performance. Post-injury performance was tested at 1 dpi, 3 dpi, 5 dpi, (cohort 1 + cohort 2) 14 dpi and 30 dpi (cohort 2) and the longest latency to fall in two trials was taken as best performance and scored. The general locomotor activity of mice was examined in an open field test (OFT) maze (40 × 40 × 40 cm, 330–350 Lux) using a video tracking system (EthovisionXT, Noldus, Wageningen, Netherlands) before and at different time points after TBI (cohort 1: pre-OP, 1 dpi, 3 dpi, and 5 dpi; cohort 2: pre-OP, 1 dpi, 3 dpi, 5 dpi, 14 dpi, and 30 dpi). Mice were placed in the center of the arena, locomotion was recorded for 3 min, and the travelling distance was determined using EthovisionXT14 software.

2.4. Brain sectioning and histopathology

Mice were decapitated in deep anesthesia using isoflurane at 4 vol% at 5 dpi or 30 dpi. Brains were collected and frozen in powdered dry ice, stored at −20 °C, and coronal brain sections were prepared using a cryotome (HM 560 Cryo-Star, Thermo Fisher Scientific, Walldorf, Germany). Brains were cut to 12 μm thick sections at 16 consecutive levels and collected in 500 μm intervals on glass slides (Superfrost Plus) from Bregma + 3.14 mm to −4.36 mm. Brain tissues from intermediate

sections (60 μm, 8 × 4) were collected from Bregma + 0.64 mm to −2.86 mm, cut along the midline to separate the ipsilesional and contralateral hemispheres, and upper quadrants of the sections containing the lesioned and perilesional brain tissue (cortex, striatum, dorsal hippocampus, thalamus) were collected (Supplementary information, Fig. S3), frozen with liquid nitrogen, and processed for RNA and/or protein extractions and RNA-sequencing.

Cresyl violet staining was carried out to perform brain volumetry and to determine the structural brain damage. Briefly, brain sections were 60 min air-dried, rehydrated for 2 min in 70 % ethanol, and stained for 10 min with a cresyl violet solution (10 mg/ml, 20 % Ethanol, Merck). Sections were washed in distilled water, dehydrated, hyalinized and mounted. Hematoxylin-Eosin (H&E) staining was performed to assess the area of hematoma according to standard protocols. Briefly, brain sections were air-dried and sequentially rehydrated, stained with H&E solution (Morphisto), dehydrated, hyalinized and then mounted.

For immunohistochemistry, brain cryosections were air-dried for 30 min, fixed for 10 min in 4 % PFA and incubated in blocking solution (5 % goat serum, 0.5 % bovine serum albumin, and 0.1 % Triton X-100 in PBS) for 60 min at RT. Primary antibodies were diluted in blocking solution and applied at 4 °C overnight. After extensive washing in PBS, highly cross-adsorbed secondary antibodies were diluted in blocking solution 1:500 and applied for 60 min. Afterwards, sections were washed with PBS, counterstained with 4′,6-Diamidino-2-phenyl-indol -dihydrochlorid (DAPI, 1:10.000, Sigma-Aldrich) and mounted. Primary, secondary antibodies, and dilutions are provided as Supplementary information (Table S4).

TdT-mediated dUTP-biotin nick end labeling (TUNEL) combined with immunohistochemistry was used to identify apoptotic cells. Brain cryosections were air dried, fixed in 4 % PFA for 20 min, rinsed in 0.1 % sodium citrate solution containing 0.1 % Triton X-100 and 3 % H_2O_2, washed in PBS, and incubated with TUNEL solution (#11684809910, Roche, Mannheim, Germany) in a water bath for 60 min at 37 °C. After 3 washes in PBS, the sections were blocked, incubated with primary antibodies specific to CD68 and NeuN, respectively, and processed as described above.

2.5. Histopathological analyses

Sections stained with cresyl violet or H&E were imaged using a bright field microscope (Stemi 305, Zeiss). Quantification of lesion volume, hippocampal granule cell layer (GCL) thickness or length, and dorsal hippocampal area were carried out using Zen software (Zeiss, RRID:SCR_013672), hematoma area was determined using ImageJ software (RRID: SCR_003070). Brain lesion volume and brain tissue loss were defined as the area lacking violet staining and the lesion volume was quantified by outlining the non-stained or missing tissue on the injured hemisphere (Villapol et al., 2012) and summation of lesion regions from 16 sections multiplying the intervals between two sections (500 μm). The relative lesion volume at 5 dpi or brain tissue loss at 30 dpi was calculated by dividing the lesion volume by the total ipsilateral hemisphere volume (Villapol et al., 2012), calculated from 16 sections as described above.

GCL thickness was measured at 5 dpi in the dorsal hippocampus between Bregma levels −1.2 mm to −1.8 mm on two sections along the suprapyramidal blade (Hummel et al., 2020). At 30 dpi, GCL length instead of thickness was used because of long-term changes of hippocampus morphology. The dorsal hippocampal area was determined on three sections (distance 500 μm) from Bregma levels −1.06 mm to −2.16 mm according to Paxinos and Franklin's mouse brain atlas. Values are expressed in % relative to the contralesional GCL or hippocampus, respectively.

Immunohistochemical images were captured using a confocal scanning microscope (LSM Examiner, Zeiss) by investigators blind to experimental randomization using identical acquisition parameters for each staining combination. Quantitative assessments were done with Image J (ImageJ, RRID:SCR_003070) with adequate threshold setting followed by the "analyze particle" plugin. Manders' colocalization coefficients were determined to analyse the overlap of IL-1β immunolabelling with CD68 or GFAP immunolabelling using the ImageJ plugin JACoP and adequate threshold settings.

2.6. Immunoblotting

Brain tissue samples collected during cryosectioning were homogenized using ice-cold RIPA buffer [50 mM Tris-HCl, pH 7.5, 150 mM NaCl, 1 mM EDTA, 1 % (v/v) NP-40, 0.1 % (v/v) sodium dodecyl sulfate, complete protease inhibitors (Roche)] and Lowry protein assay (BioRad) was used to quantify protein concentrations. For western blotting, 30 μg protein for each sample was separated by SDS-PAGE (12 %) and transferred to nitrocellulose membranes (Perbio Science). Membranes were blocked in 2.5 % skim milk for 60 min at RT, incubated with primary antibodies at 4 °C overnight, and secondary infrared dye-conjugated antibodies diluted 1:15,000 in blocking solution at RT for 60 min. Primary and secondary antibodies and dilutions are provided in the Supplementary information (Table S4).

Protein bands and optical densities were revealed and quantified using the near-infrared laser scanning Odyssey SA Imaging System device and Image Studio software (LI-COR, RRID: SCR_014579). IgG dot blots were used to evaluate BBB integrity essentially as described (Hummel et al., 2021). Briefly, proteins lysed in RIPA buffer (2 μl per dot, 1 μg/μl) were dropped onto nitrocellulose membrane, incubated with goat anti-mouse IgG IRDye800CW (1:15,000, LI-COR Biosciences, Cat#827–08364, RRID:AB_10793856), and the fluorescent signal was detected and analyzed as described above.

2.7. Gene expression analysis

Brain samples were collected as described in section 2.4 and gene expressions were quantified using a target specific standard curve of mRNA copies (Thal et al., 2008). RNeasy and QuantiTect Reverse Transcription Kits (Qiagen) were used for mRNA extraction and cDNA synthesis. SYBRgreen Kit and Maxima Hot Start Kit (Scientific) with primer and probes were used for quantitative polymerase chain reaction (qPCR) analysis (Light Cycler480, Hoffmann-La Roche AG RRID: SCR_012155) and 1 μg cDNA was used for each target per reaction in duplicate. Absolute values of gene expression were quantified and then normalized to absolute value of the reference gene cyclophilin A (PPIA). Sequences of applied primer pairs are provided in the Supplementary information (Table S5).

2.8. RNA sequencing and analysis

Total RNA of brain samples were acquired from cryosections as described in section 2.4 containing lesioned and perilesional regions (cortex, striatum, dorsal hippocampus, thalamus, Supplementary information, Fig. S3). Total RNA was purified using RNAeasy Kit (Qiagen), the quantity was assessed with the Qubit 2.0 and quality was checked using a RNA 6000 Nano chip on Agilent's bioanalyzer. Barcoded mRNA seq libraries were prepared from 400 ng total RNA using a NEBNext® Poly(A) mRNA Magnetic Isolation Module and NEBNext® Ultra™ II RNA Library Prep Kit for Illumina® with a final amplification of 12 cycles. Library concentrations were quantified using Invitrogen's Qubit HS DNA assay and average library size was analyzed on Agilent's 2100 Bioanalyzer using a HS DNA chip. Sequencing was performed at Novogene (Cambridge, UK) on an Illumina NovaSeq 6000 sequencing system using a sequencing depth of 30 Mio paired end (150 cycles) reads per sample. Sample quality was assessed with demultiplexed fastq.gz files. Sequenced reads were trimmed for adapter sequences and processed using Qiagen's software CLC Genomics workbench (v21.0.5) with CLC's default settings for RNASeq analysis. Reads were aligned to GRCm38 genome (Waterston et al., 2002), using a minimum read length of 50 bp.

The expression value unit is TPM. Results were displayed with ArrayStar 17 (Lasergene) including the number of mapped reads, target length, source length and position, strand, genes and gene IDs, annotated according to the mm10 assembly. Genes were filtered for at least 7 valid values out of 20 samples with normalized reads > 0.1 to exclude low expression genes. Data were log2 transformed, and results were displayed as scatter plots, MA-plots and Volcano plots. The P value was set at 0.05 and adjusted according to the False Discovery Rate (FDR). The q-value was set at 0.1. Hierarchical clustering was employed to assess gene expression patterns using Euclidean distance metrics. Results were displayed as heat maps with dendrograms.

Key regulated genes (based on P-value, fold change and abundance) were further analysed for gene ontology annotation enrichments using the web tool Gorilla (http://cbl-gorilla.cs.technion.ac.il/) (Eden et al., 2009) and gene set enrichment analyses (GSEA) (https://www.gsea-msigdb.org) (Subramanian et al., 2005) to assess functional implications of up- or downregulated genes and to obtain a gene ranking and heat map of the leading edge 50 up- and downregulated genes. GSEA ranked gene lists are based on fold difference and P value. RNAseq data have been deposited as GEO dataset with the provisional accession number GSE196121.

2.9. Statistical analysis

Data were analysed using GraphPad Prism software (version 9.0). Data distribution was analysed by Shapiro-Wilk normality test and QQ plots and outliers were identified by Rout's test as specified in the figure legends. Two-way ANOVA was used for multiple group comparisons (followed by Holm-Šídák post hoc test) and groups of male and female mice were analysed separately (Fig. 1, Fig. 2, Fig. 4B, Fig. 5C, Fig. 6G, H, Fig. 7). Pairwise comparisons of parametrically distributed values from histopathological analyses including only TBI mice were analysed by Student's unpaired two-tailed *t* test or the Welch's *t* test depending on SD variance, non-parametrically distributed values were analysed by Mann-Whitney *U* test (Fig. 3, Fig. 4D, Fig. 6C-E). Behavioral data of NSS, RR and OFT from pre-op, 1 dpi, 3 dpi, and 5 dpi were pooled from cohort 1 and cohort 2, while data of 14 dpi and 30 dpi were from cohort 2 only, and two-way ANOVA with mixed effect analyses followed by Holm-Šídák post hoc test, were applied due to the unequal sample size at different time-points (Fig. 8). Linear correlations between two sets of data were performed using the Pearson correlation coefficients (Fig. 4E, F, Fig. 5D, E) and the Manders' colocalization coefficients was calculated using the ImageJ plugin JACoP (Fig. 5C). Data points for individual animals are shown as mean ± SEM, $p < 0.05$ was considered statistically significant. Full statistics are reported in the Supplementary information (Table S1-S3 and Table S6-S15).

3. Results

3.1. CSF1R inhibition attenuates M/M accumulation in the early phase of TBI

Male and female mice were subjected to the CCI model of TBI or sham procedure and were fed with either the CSF1R inhibitor PLX3397 chow (290 mg/kg) or vehicle chow (Elmore et al., 2014) for 5 days (Fig. 1A). No major differences were observed in food consumption between TBI PLX3397 vs TBI vehicle groups over the 5 days of drug administration, but mice of the TBI groups eat less than sham mice as determined at 1 dpi (Supplementary information, Fig. S1, Table S2). Body weight curves showed an initial reduction after TBI that normalized over 5 days in both the PLX3397 and vehicle chow-fed groups (Supplementary information, Fig. S2, Table S3).

At 5 dpi, both $CD68^+$ M/M and $GFAP^+$ astrocytes were markedly increased at perilesional sites (Fig. 1B) compared to corresponding sites from sham animals (Fig. 1C). CSF1R inhibition by PLX3397 reduced the number of $CD68^+$ M/M by approximately 50 % in male and 35 % in female mice, and the number of $Iba1^+$ M/M by approximately 50 % both in male, and female mice, as compared to the corresponding vehicle treatment groups (Fig. 1D, Supplementary information, Fig. S4, Table S6). The number of $GFAP^+$ astrocytes in TBI or sham mice was not affected by PLX3397 treatment (Fig. 1E).

To further characterize the consequences of M/M attenuation in our TBI model, we examined a panel of gene expression markers for M/M, astrocytes, and apoptosis by qPCR at 5 dpi (Fig. 2, Supplementary information, Table S5 and Table S9). The TBI-induced up-regulation of the M/M markers *Cd68*, *Aif1*, *Fcgr1*, *Tnfa*, *Arg1*, *Mrc1*, *C1qa* (Fig. 2A-G) and the PLX3397 target *Csf1r* (Fig. 2H) were attenuated by approximately 50 %. The effects on *Tnfa* in males and *Arg1* in females need to be cautiously interpreted as TBI*PLX3397 interaction was not significant based on ANOVA statistics (Supplementary information, Table S9). CSF1R inhibition also decreased M/M gene marker expression in sham animals, albeit inconsistently. *Mrc1* expression was significantly reduced both in male and female sham mice whereas *Aif1* and *Csf1r* expressions were reduced only in sham males (Fig. 2F, H). The apoptosis gene marker *Bax* showed a reduced expression in male TBI mice after CSF1R inhibition but not the apoptosis marker *Casp3*. Hence, apoptosis markers were inconclusive, possibly related to peak expression of *Casp3* at earlier post-traumatic time-points in the CCI model of TBI (Yakovlev et al., 1997) (Fig. 2I, J). Conversely, expressions of *Il1b* and *Il1r1* were clearly increased after TBI but were not affected by PLX3397 treatment (Fig. 2K, L) suggesting a non-M/M source. Finally, *Gfap* expression was strongly up-regulated in response to TBI but PLX3397 treatment did not affect the expression levels of this astrocyte activation marker (Fig. 2M). Consistent with the mRNA expression and immunohistochemical data, immunoblots of brain lysates showed an approximately 50 % reduction of Iba1 protein levels (encoded by the *Aif1* gene), whereas GFAP expression was not altered after CSF1R inhibition in TBI mice (Fig. 2N-P). These results demonstrate that CSF1R inhibition by dietary administration of PLX3397 attenuates the TBI-induced M/M accumulation during the early phase of TBI.

3.2. CSF1R inhibition does not attenuate structural damage but neuronal apoptosis and M/M proliferation at 5 dpi

We next determined the brain lesion volume (Fig. 3A, B) and the thickness of the ipsilesional hippocampal GCL (Fig. 3C, D), that is a reliable neuropathological parameter for a brain damage remote of the direct injury site in our TBI model (Hummel et al., 2020; Ritter et al., 2021). Brain volumetry did not reveal a difference in the relative lesion volume between PLX3397- and vehicle-treated TBI mice (Fig. 3A, B). Likewise, the GCL thickness was diminished after TBI both in PLX3397- and vehicle-treated mice and did not differ in male or female TBI mice as compared to corresponding vehicle groups (Fig. 3C, D). Thus, CSF1R inhibition during the early phase of TBI did not affect the structural brain damage at 5 dpi. CSF1R inhibition by PLX3397 was found to trigger apoptosis of microglia *in vivo* (De et al., 2014) but our qPCR results rather showed reduced *Bax* gene expression after CSF1R inhibition in male mice (Fig. 2I). Apoptosis also occurs in neurons after TBI and contributes to secondary brain injury (Akamatsu and Hanafy, 2020). To assess the extent of apoptosis in M/M and neurons after CSF1R inhibition at 5 dpi, anti-CD68/anti-NeuN double-immunostaining along with TUNEL staining was performed (Fig. 3E-H). We found overall decreased numbers of $TUNEL^+$ cells in perilesional brain regions of PLX3397 vs vehicle treated TBI animals (Fig. 3E, F). The vast majority of $TUNEL^+$ cells expressed the neuronal marker NeuN (Fig. 3G, H). Occasionally, regardless of PLX3397 or vehicle treatment after TBI, we observed $TUNEL^+/NeuN^+$ cells in direct vicinity or engulfed with $CD68^+$ M/M suggesting the phagocytic uptake of apoptotic neurons (Fig. 3G, H, higher magnification of boxed regions). However, we found no $TUNEL^+/CD68^+$ cells devoid of NeuN immunostaining. We infer that CSF1R antagonism inhibited M/M proliferation rather than inducing apoptosis of established M/M. It is unlikely, that we missed a premature

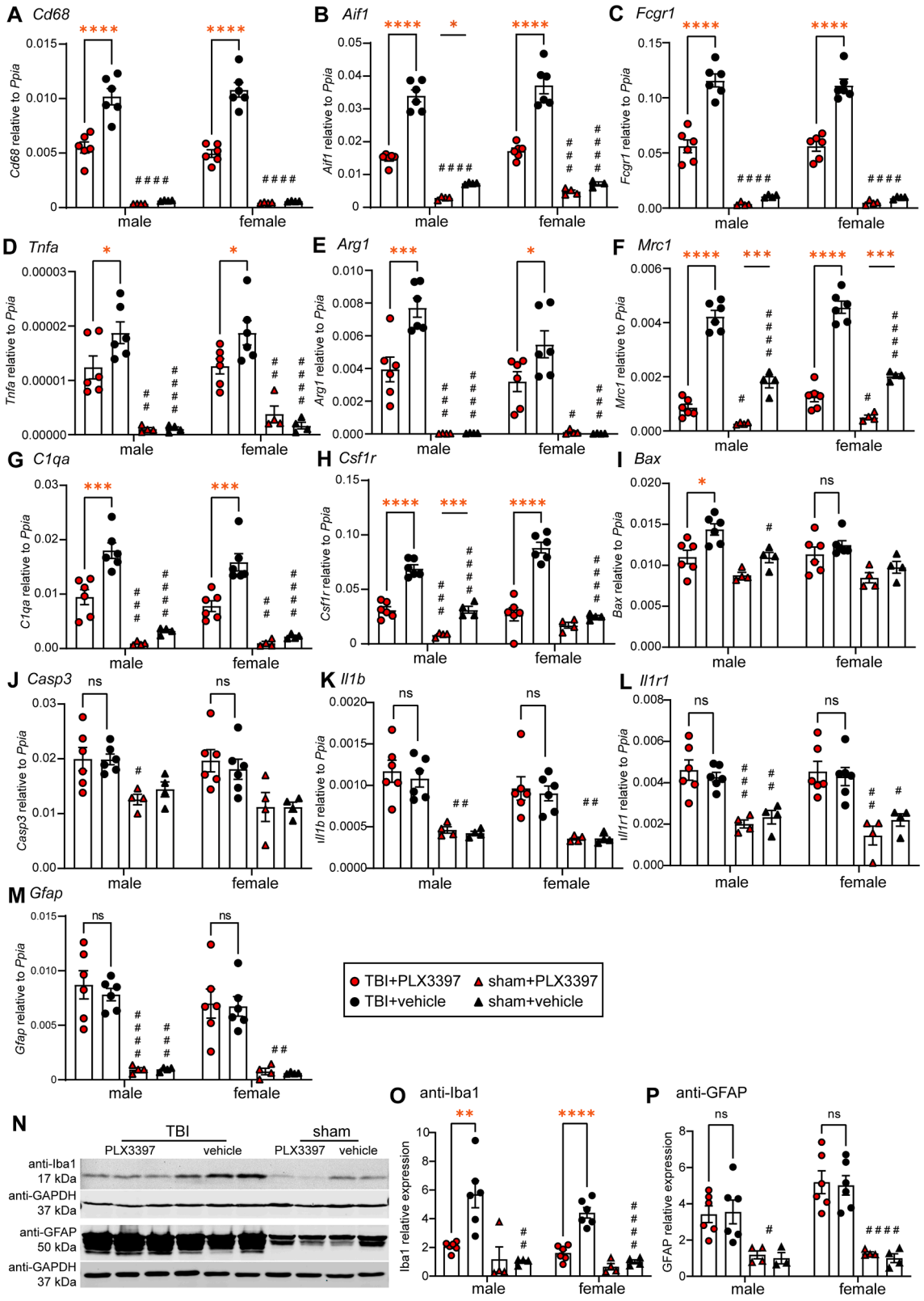

Fig. 2. CSF1R inhibition attenuates M/M accumulation in the early phase of TBI (A-M) mRNA expression of M/M, astrogliosis, and apoptosis related markers at 5 dpi. Values are expressed relative to the reference *Ppia*. TBI: n = 6 per group, sham: n = 3–4, per group. (N) Immunoblot showing expression of the M/M marker Iba1, the astrocyte marker GFAP, and the reference GAPDH. TBI-induced Iba1 expression, but not GFAP expression, was attenuated after PLX3397-treatment. (O, P) Iba1 and GFAP relative to the reference GAPDH and normalized to sham vehicle. TBI: n = 6, sham: n = 3–4, each group. Two-Way ANOVA followed by Holm Šídák's multiple comparisons test (A-M, O, P). Two sham samples were not detectable and were excluded (B, P). Values from individual animals and mean ± SEM are shown. *indicates PLX3397 vs vehicle, *p < 0.05, **p < 0.01, ***p < 0.001, ****p < 0.0001. #indicates TBI vs sham, #p < 0.05, ##p < 0.01, ###p < 0.001, ####p < 0.0001, ns = not significant.

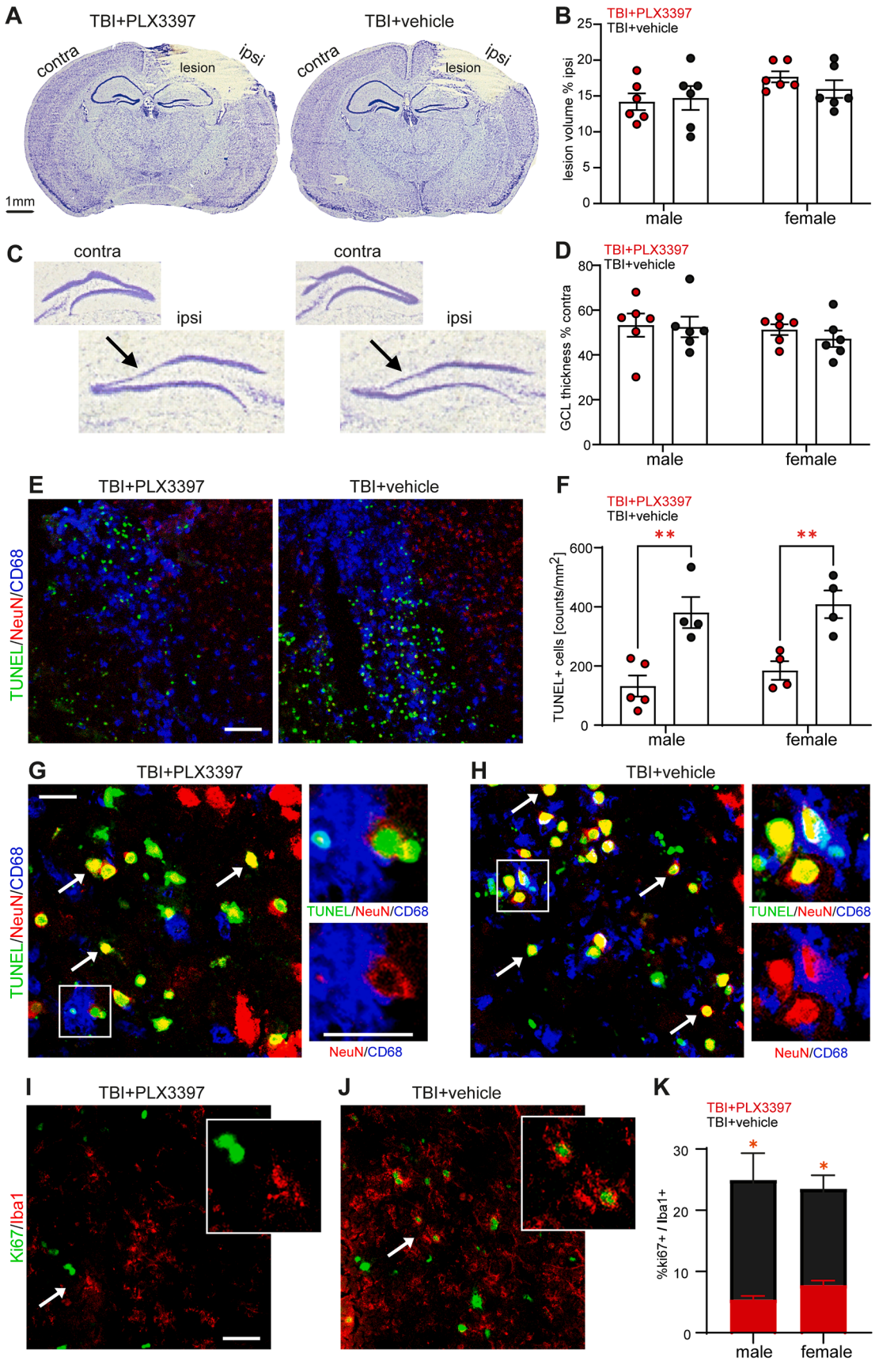

(caption on next page)

Fig. 3. CSF1R inhibition does not attenuate structural damage but neuronal apoptosis and M/M proliferation at 5dpi (A) Cresyl-violet stained sections showing structural brain damage in PLX3397 and vehicle treatment TBI groups at 5 dpi. (B) Lesion volume at 5 dpi, values (n = 6 per group) is expressed in % relative to the volume of the ipsilesional hemisphere. (C) Image enlargements showing the ipsi- and contralesional GCL of the hippocampus. Arrows point to decreased thickness of the ipsilesional GCL. (D) Ipsilesional GCL thickness in PLX3397 and vehicle treatment TBI groups (n = 6 per group). Values are expressed in % relative to contralesional GCL thickness. (E, F) Triple-fluorescent TUNEL/anti-NeuN/anti-CD68 staining showing reduced numbers of TUNEL$^+$ cells in the perilesional brain tissue in PLX3397 vs vehicle treatment TBI groups at 5 dpi (male TBI + PLX3397/+vehicle: n = 4–5; female TBI + PLX3397/+vehicle: n = 4). (G, H) Triple fluorescent TUNEL/anti-NeuN/anti-CD68 staining showing that the majority of TUNEL$^+$ cells are NeuN$^+$ neurons (white arrows). Image enlargements from boxed regions show engulfment of TUNEL$^+$ neurons by CD68$^+$ M/M. (I, J) anti-Ki67/anti-Iba1 immunostaining in the ipsilesional brain tissue of TBI + PLX3397 vs TBI + vehicle groups. Arrows point to cells shown in image enlargements. (K) Histogram showing a lower percentage of Iba1$^+$ cells expressing Ki67 cells in PLX3397 vs vehicle treated TBI groups (male TBI + PLX3397/+vehicle: n = 5–6, female TBI + PLX3397/+vehicle: n = 6), Student's unpaired two-tailed *t* test or Welch's *t* test (B, D, F, K). One outlier was identified by Rout's test and excluded (K). Values from individual animals and mean ± SEM are shown. *indicates PLX3397 vs vehicle, *p < 0.05, **p < 0.01. Scales: 1 mm (A), 100 μm (E, I, J), 50 μm (G, H), 25 μm (G, H enlargements). (For interpretation of the references to colour in this figure legend, the reader is referred to the web version of this article.)

fast on– and offset of apoptosis in the PLX3397 group that was finished before 5 dpi. To examine proliferation, perilesional brain regions from TBI animals were examined after double-immunostaining for the M/M marker Iba1 and the proliferation marker Ki67 (Fig. 3I, J). Indeed, CSF1R antagonism inhibited M/M proliferation. The percentage of Iba1$^+$ cells expressing Ki67 cells was strongly reduced both in male and female mice (Fig. 3K). Hence, CSF1R inhibition did not affect structural brain damage but attenuated neuronal apoptosis and M/M proliferation during the early phase of TBI.

3.3. M/M attenuation compromises brain tissue clearance during the early phase of TBI

The absence of beneficial effects on structural brain damage after CSF1R inhibition may result from the dual role of M/M in TBI. M/M actions such as phagocytosis may have beneficial effects on neuronal survival (Herzog et al., 2019; Lan et al., 2017) but may also exacerbate BBB and brain tissue damage (Haruwaka et al., 2019; Jolivel et al., 2015). We therefore assessed BBB integrity and intracerebral hematoma after TBI. Anti-mouse IgG dot blots using protein lysates from injured hemispheres demonstrated increased amounts of IgG as a proxy of IgG extravasation after BBB damage (Fig. 4A) but no differences were detected between PLX3397 and vehicle TBI mice (Fig. 4B). Intracerebral hematoma visualized by H&E staining showed that hematoma were restricted to the damaged ipsilesional brain tissue and were apparently increased following M/M reduction via CSF1R inhibition (Fig. 4C). This was confirmed by quantification of the hematoma area in consecutive sections (Fig. 4D). Since the clearance of intracerebral hematoma involves microglia (Lan et al., 2017), we asked whether reduced numbers of M/M in CSF1R antagonized mice may compromise hematoma removal. In agreement with this hypothesis, hematoma area was negatively associated both with *Cd68* mRNA expression or counts of perilesional CD68$^+$ M/M (Fig. 4E, F). Thus, M/M attenuation after CSF1R inhibition did not affect BBB integrity but compromised brain tissue clearance resulting in larger intracerebral hematoma areas at 5 dpi.

3.4. Pro-inflammatory IL-1β expression persists despite reduction of M/M in the early phase of TBI

CSF1R inhibition reduced M/M accumulation along with the gene expression of several M/M markers at 5 dpi (Fig. 2). However, gene expressions of pro-inflammatory IL-1β and the corresponding receptor IL-1R1 were not affected by M/M attenuation (Fig. 2 K, L). As IL-1β is strongly induced after brain injury and negatively impacts clinical outcomes of TBI (Alam et al., 2020; Bodnar et al., 2021), we sought to clarify the cellular origin of IL-1β in our TBI model (Fig. 5). Triple-immunostaining using antibodies specific to IL-1β, CD68, and GFAP followed by co-localization analyses (Fig. 5A-C) revealed that anti-IL-1β immunoreactivity was predominantly localized to GFAP$^+$ astrocytes but not to CD68$^+$ M/M. In addition, correlation analyses showed that *Il1b* mRNA expression was positively associated with *Gfap* mRNA expression (Fig. 5D), but not with *Cd68* mRNA expression (Fig. 5E). These results suggest IL-1β expression predominantly in astrocytes that was therefore able to withstand the M/M attenuation in the early phase of TBI.

3.5. Early CSF1R inhibition improves long-term brain tissue maintenance with subtle regional sex-specific differences

To study long-lasting effects of early CSF1R inhibition, the second cohort of mice was subjected to TBI and dietary PLX3397 administration for 5 dpi, followed by discontinuation of drug treatment up to sacrifice at 30 dpi, a time point regarded as chronic phase (Fig. 6A). Anti-CD68/anti-GFAP double-immunostaining confirmed ongoing inflammatory activity and astroglial scar formation in the perilesional brain tissue as well as repopulation of the perilesional brain tissue by M/M (Supplementary information, Fig. S5). Histological examination by cresyl violet staining at 30 dpi showed brain tissue loss and the formation of a lesion cavity, which extended into the hippocampus that showed an atrophic appearance including the GCL (upper arrow in Fig. 6B) as compared to the contralesional hemisphere (Fig. 6B). The relative brain tissue loss was reduced after early CSF1R inhibition, both in male and female mice, showing that early PLX3397 treatment improved long-term brain tissue maintenance (Fig. 6C). GCL length measurements revealed a better preservation of the GCL in the ipsilesional hippocampus both in PLX3397-treated TBI male and female mice as compared to vehicle mice (Fig. 6D). Similarly, the dorsal hippocampal area was larger in PLX3397- vs vehicle-treated TBI mice, however, this difference was significant in male mice only (Fig. 6E). Cresyl violet-stained brain sections also showed increased cell density in the ipsilesional thalamus (lower arrow in Fig. 6B). Infiltration of this remote area of the primary injury and lesion cavity site by M/M and neurodegeneration are long-lasting features of the CCI model of TBI in rats (Donat et al., 2016; Glushakov et al., 2018). Therefore, we performed anti-CD68/anti-NeuN double-immunostaining and counted M/M and neurons in the ipsilesional and contralesional thalamus from TBI animals (Fig. 6F-H). In the ipsilesional thalamus from TBI animals, the number of CD68$^+$ M/M was strikingly increased, while the number of neurons was strongly decreased compared to the contralesional thalamus (Fig. 6G-H). Early CSF1R inhibition by PLX3397 reduced the numbers of CD68$^+$ M/M and increased numbers of NeuN$^+$ neurons at this chronic stage of TBI. The differences reached statistical significance in male but not in female mice (Fig. 6G, H). Taken together, early CSF1R inhibition after TBI improved long-term brain tissue maintenance with subtle regional sex-specific differences.

3.6. Early CSF1R inhibition after TBI results in sex-specific long-term change in candidate marker genes

Next, we performed gene expression analyses by qPCR at 30 dpi using the same set of markers as at the early time-point at 5 dpi (Fig. 7A-M, Supplementary information, Table S5 and Table S14). The results revealed M/M repopulation of the injured brain after early CSF1R inhibition. The vast majority of candidate marker genes were still strongly increased in TBI vs sham indicating ongoing inflammation. Some candidates were still lower in PLX3397-treated male TBI mice as compared

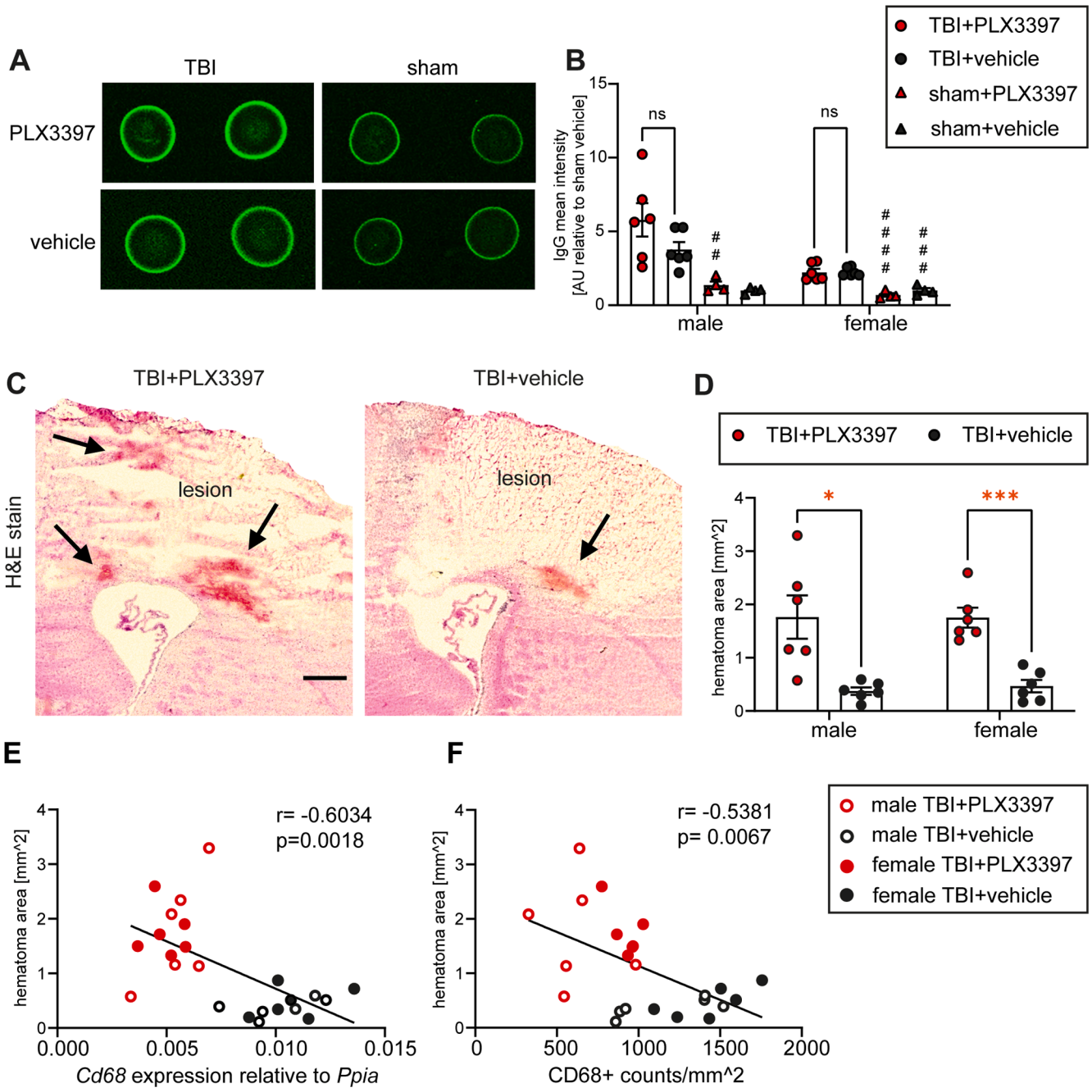

Fig. 4. M/M attenuation compromises brain tissue clearance during the early phase of TBI (A) anti-IgG dot-blots showing increased IgG in brain lysates from ipsilesional TBI vs sham at 5 dpi. (B) IgG intensities, values are expressed relative to sham vehicle (TBI: n = 6, sham: n = 4, per group) (C) H&E staining showing intracerebral hematoma (arrows) in the ipsilesional brain tissue of TBI + PLX3397 and TBI + vehicle groups. (D) The hematoma area is increased in TBI + PLX3397 vs TBI + vehicle (n = 6 per group). (E, F) Linear correlation analysis by Pearson correlation coefficients showing a negative correlation between *Cd68* expression or $CD68^+$ M/M counts and hematoma area (n = 6 per group). Two-Way ANOVA followed by Holm Šídák's multiple comparisons test (B), Student's unpaired two-tailed *t* test or Welch's *t* test (D). Values from individual animals and mean ± SEM are shown. *indicates PLX3397 vs vehicle, ***$p < 0.001$. # indicates TBI vs sham, ##$p < 0.01$, ###$p < 0.001$, ####$p < 0.0001$. Scale: 500 μm (C).

to vehicle treatment, whereas such differences were not observed or oppositely regulated in PLX3397 treated female TBI mice. Specifically, this applied to the M/M marker *Cd68*, *Mrc1* (Fig. 7A, F), the apoptosis markers *Bax* and *Casp3* (Fig. 7I, J), and the astrocyte marker *Gfap* (Fig. 7M), and to *Il1b* and *Il1r1* (Fig. 7K, L). However, TBI*PLX3397 interaction based on ANOVA statistics was insignificant for *Mrc1* and *Bax in males*, and for *Gfap* in males and females, which requires cautious interpretation for the attenuated up-regulation of these genes after TBI and PLX3397 treatment (Supplementary information, Table S14). Overall, the results suggested that early CSF1R inhibition after TBI resulted in sex-specific long-term changes and long-lasting benefits for males, but rather not for females.

3.7. Early CSF1R inhibition results in subtle short- and long-term changes in neurological outcome

Time-courses of neurological deficits were assessed using a neurological severity score (NSS), the rotarod test, and the open field test (OFT) (Fig. 8). Consistent with previous findings in our TBI model, the NSS reached a peak at 1 dpi and decreased from 1 dpi to 30 dpi in all TBI

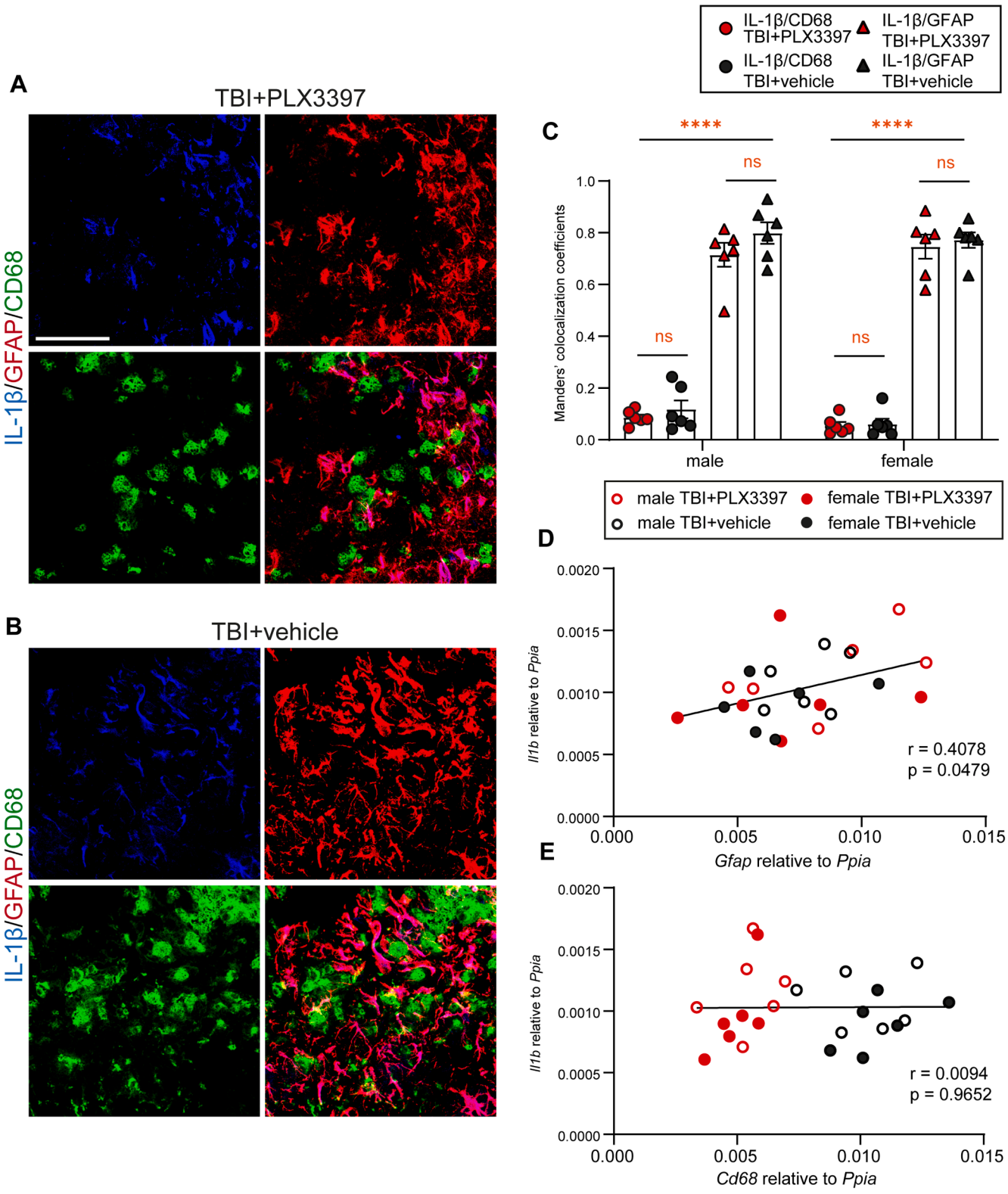

Fig. 5. Pro-inflammatory IL-1β expression persists despite M/M reduction in the early phase of TBI (A, B) IL-1β/CD68/GFAP triple-immunostaining in the perilesional brain tissue at 5 dpi showing that IL-1β is rather localized to GFAP$^+$ astrocytes than CD68$^+$ M/M. (C) Mandeŕs colocalization coefficients showing strong IL-1β overlap with GFAP$^+$ astrocytes but not with CD68$^+$ M/M, n = 6 per group. (D) Linear correlation analysis by Pearson correlation coefficients showing positive correlation between *Il1b* and *Gfap* expression (n = 6 per group). (E) Linear correlation analysis by Pearson correlation coefficients showing no correlation between *Il1b* and *Cd68* expression (n = 6 per group). Two-Way ANOVA followed by Holm Šídák's multiple comparisons test (C). Values from individual animals and mean ± SEM are shown, *indicates IL-1β/CD68 compared to IL-1β/GFAP, ****p < 0.0001, ns = not significant. Scale: 50 μm (A, B).

groups (Hummel et al., 2020). NSS remained almost zero throughout the time-course in sham mice (Fig. 8A, B). The NSS was lower in PLX3397-treated male TBI mice at 1 dpi and 3 dpi as compared to the corresponding vehicle-treated mice but the benefit was not maintained at later time-points. In female TBI mice, CSF1R inhibition had no effect in the early phase and worsened the NSS in the chronic phase of TBI at 30 dpi as compared to vehicle (Fig. 8B). In the rotarod test, there was no difference between PLX3397- and vehicle-treated male TBI mice

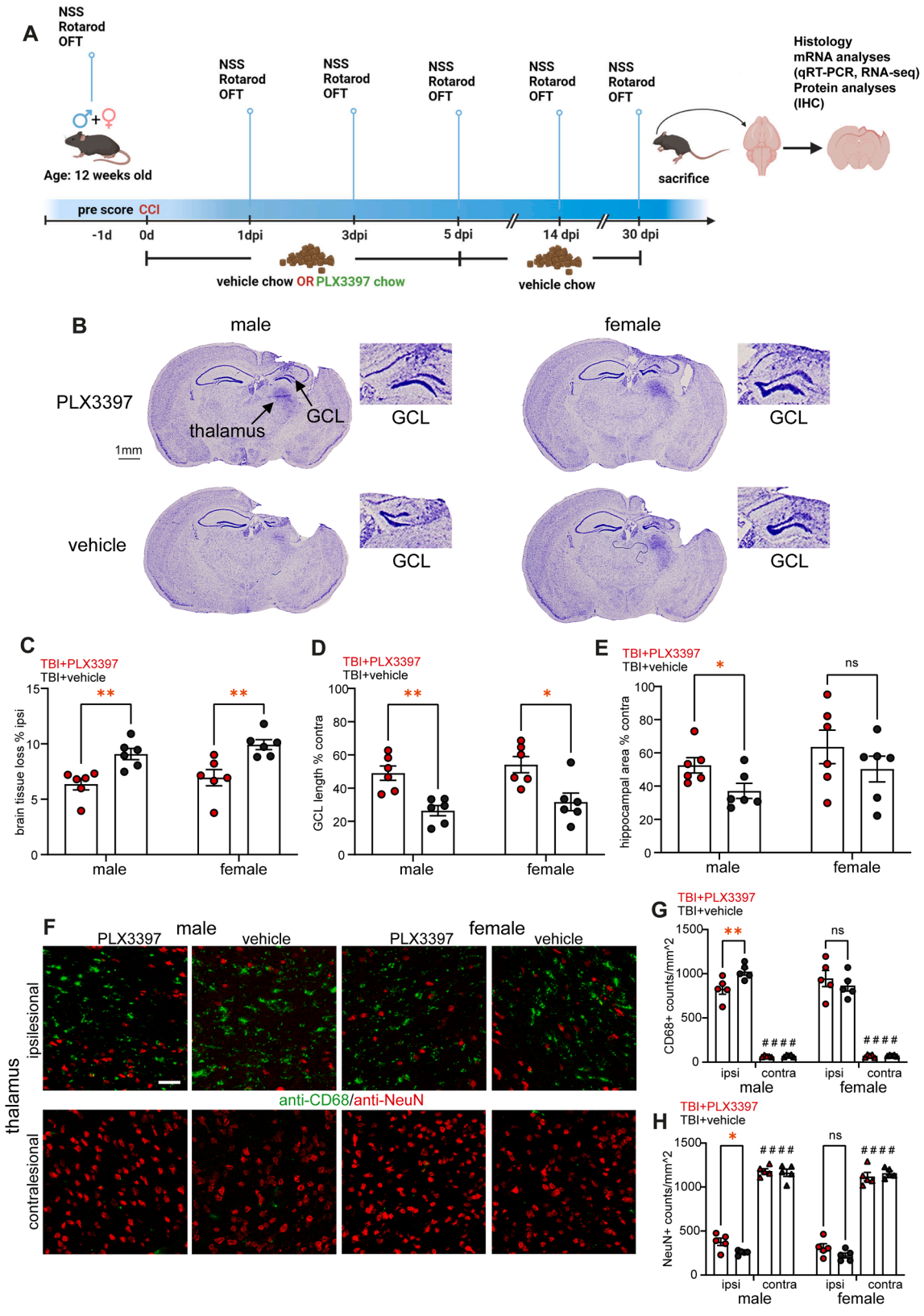

(caption on next page)

Fig. 6. CSF1R inhibition during the early phase of TBI improves long-term brain tissue maintenance (A) Experimental design of 30 days survival groups (cohort 2, equal sex ratio). Neurological Severity Score (NSS), rotarod performance (RR) and open field test (OFT) were conducted 1 day before TBI, at 1, 3, 5, 14, and 30 dpi. PLX3397 (290 mg/kg body weight) or vehicle chow was administered for 5 days and then exchanged to vehicle chow until 30 dpi. After a survival time of 30 days, brains were processed for histology, mRNA and protein analyses. (B) Cresyl-violet staining of sections showing brain tissue loss at 30 dpi. Arrows point to the ipsilesional GCL and to a high cell density area in the thalamus, respectively. Image enlargements showing the ipsilesional GCL of the hippocampus in PLX3397 vs vehicle TBI groups. (C) Brain tissue loss at 30 dpi, values (n = 6 per group) are expressed in % relative to the volume of the ipsilesional hemisphere. (D) Ipsilesional GCL length in PLX3397 vs vehicle treatment TBI groups (n = 6 per group), values are expressed in % relative to contralesional GCL length. (E) Ipsilesional dorsal hippocampal area in PLX3397 vs vehicle treatment TBI groups (n = 6 per group), values are expressed in % relative to contralesional hippocampal area. (F) anti-CD68/anti-NeuN immunostaining showing M/M infiltration of the ipsilesional thalamus and neurodegeneration, which were not observed in the contralesional thalamus. (G, H) Histograms showing reduced numbers of $CD68^+$ M/M in male PLX3397- vs vehicle-treatment TBI groups (n = 5 per group). Student s unpaired two tailed *t* test or Mann-Whitney *U* test (C, D, E). Two-Way ANOVA followed by Holm Šídák s multiple comparisons test (G, H). Values from individual animals and mean ± SEM are shown. *indicates PLX3397 vs vehicle, *$p < 0.05$, **$p < 0.01$, # indicates TBI vs sham, ####$p < 0.0001$, ns = not significant. Scale: 1 mm (B), 50 μm (F). (For interpretation of the references to colour in this figure legend, the reader is referred to the web version of this article.)

(Fig. 8C), but again, PLX3397 worsened motor deficits in female TBI mice (Fig. 8D). In the OFT, we did not observe any effects of TBI and CSF1R inhibition during the early phase of TBI from 1 dpi to 5 dpi (Fig. 8E, F). PLX3397-treated TBI males were somewhat less active than the vehicle comparators (Fig. 8E) while female TBI mice showed a tendency to increased activity (Fig. 8F). Overall, CSF1R inhibition had rather subtle short- and long-term effects on behavioral readouts without convincing evidence for an improvement of neurological outcome.

3.8. *Transcriptomic profiles indicate that early CSF1R inhibition improves long-lasting neuronal maintenance and recovery*

To better characterize long-term changes at the molecular level, we studied global transcriptomes by RNAseq analysis and compared TBI mice treated with PLX3397 or vehicle, 10 mice per group, each consisting of 5 males and 5 females. Therefore, analyses were done with all mice to reveal drug effects, and further analyses compared males and females separately to reveal sex differences of drug responses, M/M attenuation and repopulation (Fig. 9). Top 16 genes according to P/q-value included prominent synaptic genes (*Tmem132d, Prkcz, Camk2a, Fam163b, Brinp1, Pip4k2c, Ptk2b, Lrrc4*) (Fig. 9A, Supplementary information Fig. S10 shows top 50 regulated genes). GSEA revealed leading edge differentially expressed genes (Fig. S6) in PLX3397-treated TBI mice as compared to vehicle TBI mice and enriched gene sets of spine morphogenesis, synaptic vesicle exocytosis, and glutamate receptor signaling, postsynaptic membrane, among other similar terms (Supplementary information Fig. S7 and Fig. S8). Genes involved in oxidative phosphorylation, oxidoreductase processes and ribosomal structures were enriched in vehicle treated mice (Supplementary information Fig. S7 and Fig. S9).

The data suggest that M/M reduction and repopulation via early CSF1R inhibition improved neuronal maintenance and recovery particularly at the level of synapses. Oppositely, high oxidative phosphorylation plus high ribosomal biogenesis in vehicle-treated TBI mice suggest increased abundance of metabolically highly active immune or glial cells. Comparisons of males and females separately shows an expected loss of significance owing to lower sample sizes (Fig. 9A). Key candidates *Tmem132d* and *Prkcz* were upregulated in both sexes (Fig. 9B, C), among others (Fig. 9D). The loss of overall significance was stronger in females than males (Fig. 9A) suggesting that males benefited more from the treatment at this late time point at 30 dpi. Indeed, further comparisons of genes which were differentially regulated in females but not in males were involved in immune processes, phagocytosis and related gene ontology terms. Comparisons of PLX3397-treated female vs male mice revealed higher expression of extracellular signalling molecules or receptors such as CD36, clotting factors and metalloproteases and extracellular matrix components such as collagen species in female mice (Supplementary information Fig. S10 and Fig. S11). There were no comparable differences between vehicle-treated female and male mice except for few X-chromosome localized genes. Gene ontology analyses for genes which were higher expressed in PLX3397-treated female vs PLX-treated male mice showed an enrichment of GOcc "extracellular matrix" and related terms. Similar results were obtained by filtering for genes that were upregulated in female PLX3397-treated versus female vehicle-treated mice but were downregulated or not regulated in PLX-treated male over vehicle-treated male mice. The data suggest sex-specific differences of the drug response or of its persistence at this late time point of 30 dpi.

4. Discussion

This experimental study investigated short- and long-term effects of M/M attenuation during the early phase of TBI using CSF1R inhibition via PLX3397. We used a clinically relevant approach with early, short-course posttraumatic drug administration and considered sex as a biological variable. We found no early brain tissue protection despite a marked M/M reduction at 5 dpi but stronger indices of neuronal maintenance and recovery in the chronic phase of TBI, i.e. long after the drug discontinuation. The results suggest long-lasting recovery-permissive effects after early CSF1R inhibition and M/M repopulation and this therapeutic benefit was stronger in males than in females.

M/M duality after different types of CNS injuries is an accepted concept. While the removal of cell debris and dead cells by M/M helps restoration, phagocytosis may also affect viable neurons after brain injury (Neher et al., 2013), and the release of neurotoxic substances by M/M can exacerbate neuronal injury and cell death (Donat et al., 2017). Therefore, the failure of PLX3397 to attenuate early structural brain damage at 5 dpi despite M/M attenuation by around 50 % seems surprising. Either the degree of attenuation was insufficient, or the attenuation seriously impaired beneficial tissue clearance, or M/M−independent mechanisms critically contributed to the damage.

(i) Drug dose or efficacy: Owing to massive inflammatory activation post-injury, the M/M reductions might have been insufficient to achieve brain tissue protection during the acute phase of TBI. However, even this short period increased the hemorrhage. Elimination of M/M might have led to overall stronger effects including hemorrhage, but evaluation of early post-traumatic therapeutic effects using a post-traumatic treatment period of 5 days makes it impossible to simultaneously assess the efficacy of complete elimination of microglia. Hence, designs addressing short-term efficacy and designs addressing total depletion are mutually exclusive. Indeed, elimination of microglia before TBI in a model of fluid percussion injury (FPI) improved neuronal maintenance (Wang et al., 2020). However, in the same model, the pre-injury depletion of microglia prevented acute inflammatory processes but did not attenuate the model-specific axotomy of neurons (Witcher et al., 2018). Similarly, microglia depletion did not influence acute axonal degeneration after optic nerve injury and simultaneous depletion of microglia and peripheral macrophages even compromised nerve regeneration (Hilla et al., 2017).

(ii) Impairment of beneficial tissue clearance: Our results indicate that M/M attenuation during the early phase of TBI compromises beneficial tissue clearance, because we found larger intracerebral hematoma in PLX3397 treated TBI mice at 5 dpi, likely resulting from a

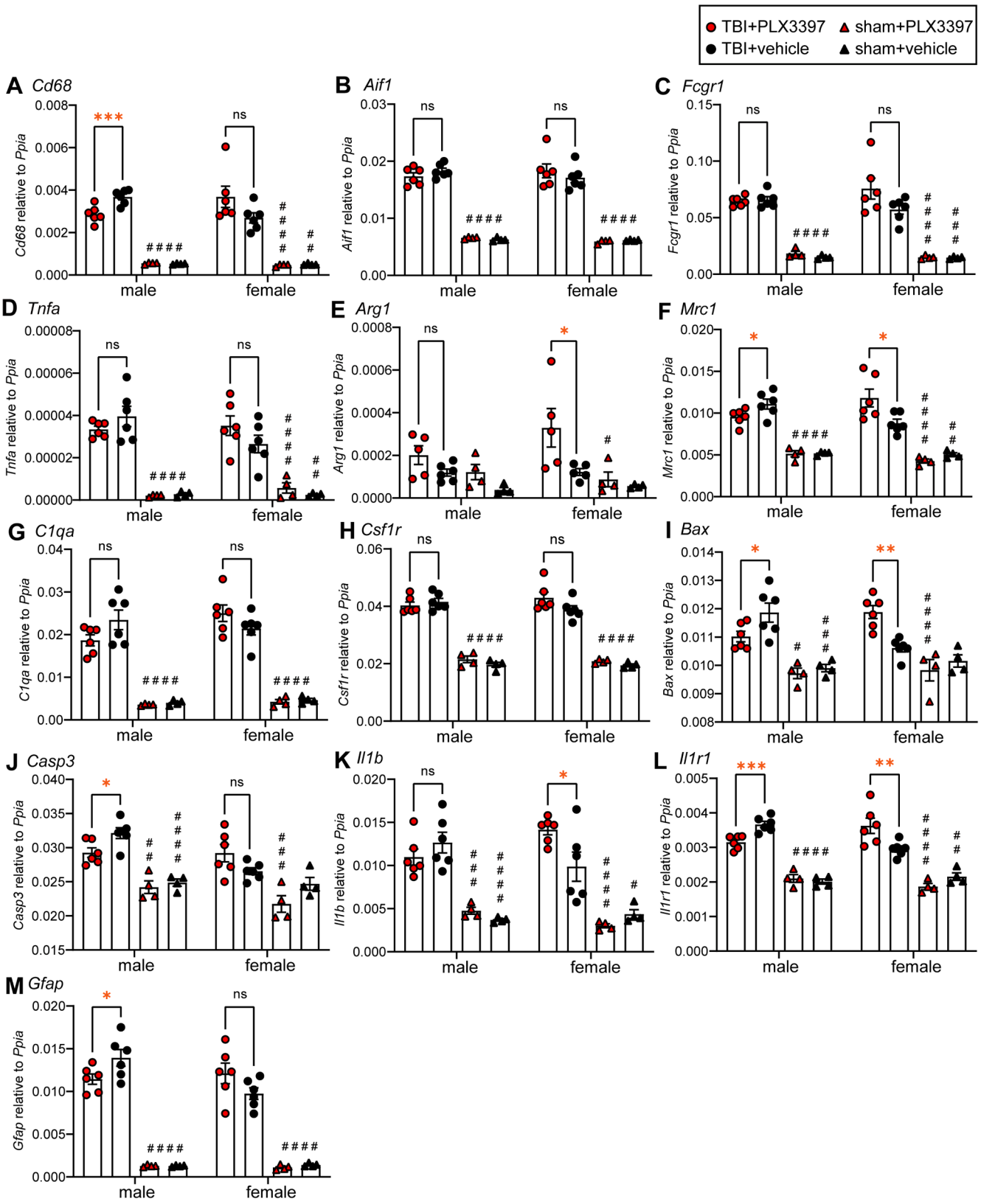

Fig. 7. Early CSF1R inhibition after TBI results in sex-specific long-term changes in candidate marker genes (A-M) mRNA expression of M/M, astrogliosis, and apoptosis related markers at 30 dpi. Values are expressed relative to the reference *Ppia*. TBI: n = 5–6 per group, sham: n = 3–4, per group. Two-Way ANOVA followed by Holm Šídák's multiple comparisons test (A-M). One sample was below detection threshold for *Arg1* assay and two outlier were identified by Rout's test and excluded (E). Values from individual animals and mean ± SEM are shown. *indicates PLX3397 vs vehicle, *p < 0.05, **p < 0.01, ***p < 0.001, ****p < 0.0001. # indicates TBI vs sham, #p < 0.05, ##p < 0.01, ###p < 0.001, ####p < 0.0001, ns = not significant.

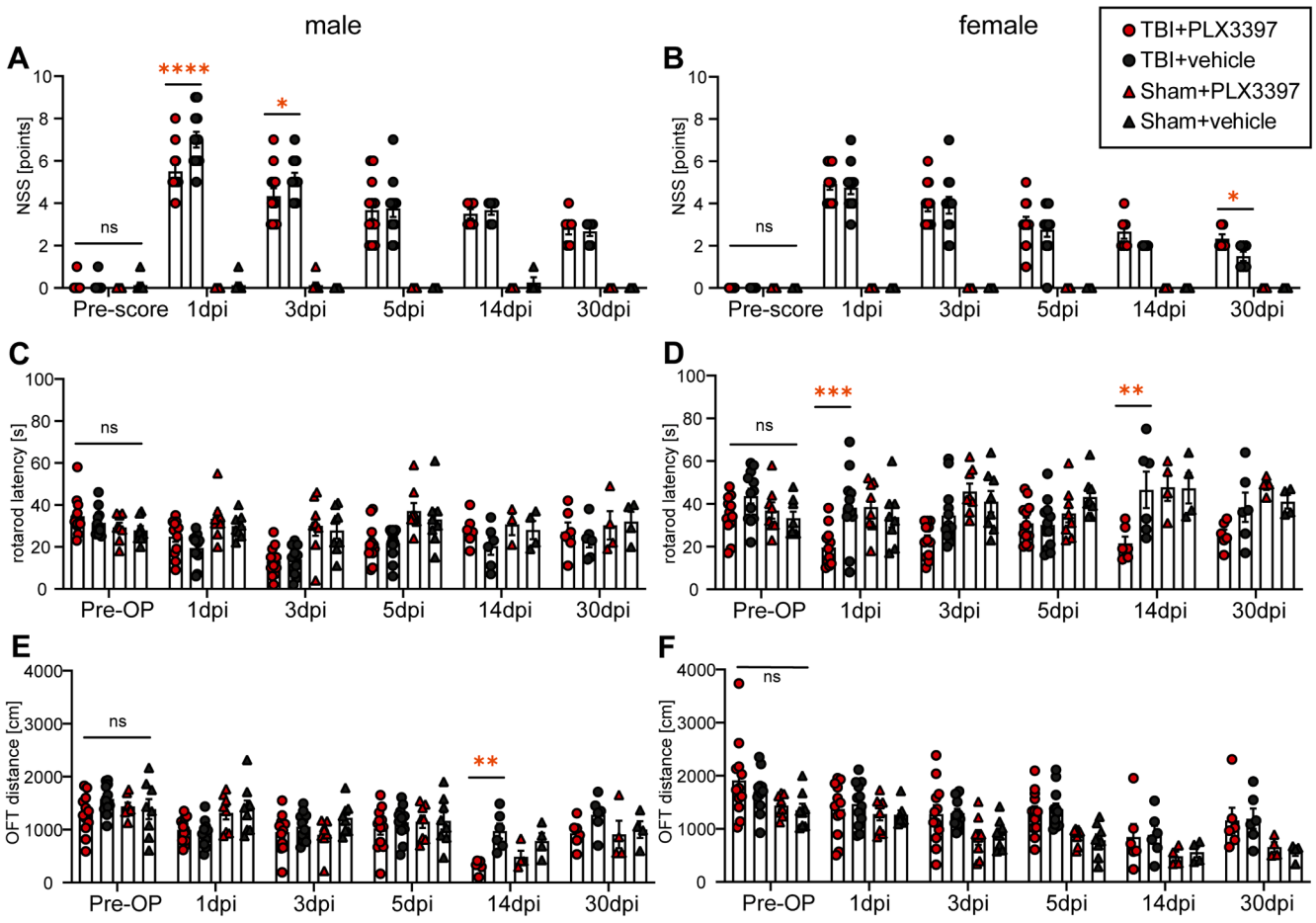

Fig. 8. Neurological outcome in behaving mice was almost not affected (A, B) NSS in male and female mice (higher scores indicate increased severity). (C, D) Rotarod performance in male and female mice (higher latency indicates better performance).TBI: n = 12 (pre-op, 1 dpi, 3 dpi, and 5 dpi), 6 (14 dpi and 30 dpi), per group, sham: n = 7–8 (pre-op, 1 dpi, 3 dpi, and 5 dpi), 3–4 (14 dpi and 30 dpi), per group. One outlier was identified by Rout's test and excluded (C, F). Two-Way ANOVA with mixed-effects model followed by Holm Šídák's multiple comparisons test (A-F). Values from individual animals and mean ± SEM are shown. *indicates PLX3397 vs vehicle, *p < 0.05, **p < 0.01, ***p < 0.001, ****p < 0.0001. ns = not significant.

failure of brain tissue and debris clearance (Brockhaus et al., 1996; Hanlon et al., 2019; Neumann et al., 2009). Brain tissue clearance critically depends on microglia (Lan et al., 2017) and we propose that the reduced numbers of M/M explains the larger intracerebral hematoma in PLX3397 treated TBI mice at 5 dpi.

We further observed that some M/M approached and internalized apoptotic neurons both in PLX3397- and vehicle-treated mice, consistent with previous findings that the phagocytic capacity of microglia is not directly dependent on CSF1R signaling (Delaney et al., 2021). Therefore, CSF1R inhibition does not impair phagocytosis *per se* and an overall M/M decrease likely explains the increased hematoma area in PLX3397-treated mice in our TBI model.

(iii) M/M−independent effects: Inflammatory mechanisms not originating from M/M can trigger injury progression during the early phase of TBI (Witcher et al., 2021). Notably, we observed that CSF1R inhibition did not affect gene expression of IL-1β and its receptor IL-1R1 despite marked M/M reduction at 5 dpi. IL-1β is strongly induced after brain injury, with negative impact on clinical outcomes of TBI (Alam et al., 2020; Bodnar et al., 2021). Consequently, anti-IL-1β antibody-mediated neutralization shows protective effects in experimental TBI (Clausen et al., 2009). M/M are a major source of IL-1β. However, in our model, using immunostaining, IL-1β was localized in reactive astrocytes in the perilesional tissue, which is in agreement with previous findings in a rat weight-drop model of TBI (Lu et al., 2005), and that IL-1β signaling in astrocytes induces neuronal cell death (Thornton et al., 2006). IL-1β immunostaining of astrocytes might be contributed by IL-1β scavenging (Bourke et al., 2003) but our results rather favor the hypothesis that astrocytes indeed generate and release IL-1β because IL-1β immunoreactivity and gene expression persisted under PLX3397 treatment and thereby contribute to neuronal injury during the early phase of TBI.

Irrespective of the failure to reduce IL-1β, CSF1R inhibition reduced neuronal cell death during the early phase of TBI. This was evidenced by decreased gene expression of the pro-apoptotic regulator Bax and reduced numbers of TUNEL^{+} neurons at 5 dpi in male TBI. However, no differences were observed for *Casp3*, possibly related to peak expression of this marker at earlier post-traumatic time-points in the CCI model of TBI (Yakovlev et al., 1997), whereas peak expression of *Bax* was observed from 4-6 dpi (Wennersten et al., 2003). Reduced neuronal apoptosis was also reported in experimental TBI at 3 dpi following pre-injury administration of PLX3397 (Wang et al., 2020), suggesting the involvement of neurotoxic M/M−derived factors such as the pro-inflammatory cytokine TNFα which was reduced in the PLX3397-treated TBI groups. TNFα is involved in neuronal apoptosis after TBI (Bermpohl et al., 2007) that was shown to trigger cell death via Bax (Guadagno et al., 2013) and synergistically promotes neuronal cell death together with IL-1β in vitro (Chao et al., 1995; Ye et al., 2013). Nevertheless, PLX3397-mediated attenuation of TNFα and Bax signaling and reduction of neuronal apoptosis after CSF1R inhibition was apparently still insufficient to reduce the structural brain damage at 5 dpi in our study. We therefore propose that impaired brain tissue clearance and persistent pro-inflammatory signaling independent of M/M may

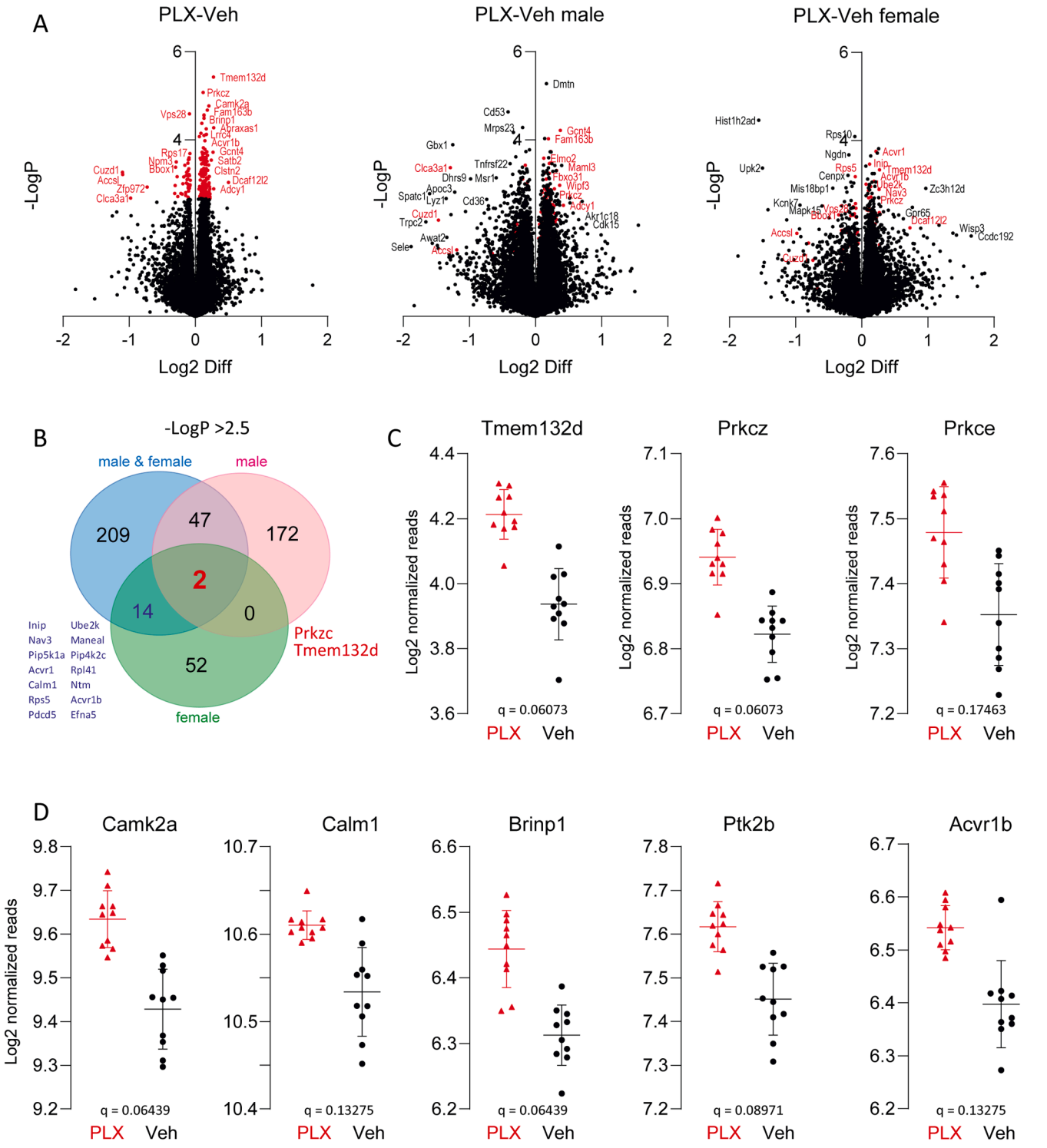

Fig. 9. Transcriptomic profiles indicate that early CSF1R inhibition improves long-lasting neuronal maintenance and recovery Mice were treated with PLX3397 (n = 5 male, 5 female) or vehicle chow (n = 5 male, 5 female) for 5 days after TBI and then with vehicle chow until 30 dpi. Brain tissue of the ipsilesional hemisphere from TBI mice (upper quadrant) was collected at 30 dpi and subjected to RNAseq analysis. (A) Volcano plots of differential gene expression in PLX3397 vs vehicle treated mice. The X-axis shows the log2 difference (i.e. fold difference). Genes reduced in PLX3397-treated mice are negative and upregulated genes positive. The Y-axis shows the negative logarithm of the P-value. The left plot included male and female mice (n = 10 per group), the middle and right panel compared males only or females only, respectively (n = 5 per group). Top 150 candidate genes according to P-value are highlighted in red. (B) VENN diagram of differentially expressed genes in PLX3397 vs vehicle treated mice (n = 10 m-f groups, male only (n = 5) and female only (n = 5). The criterion for gene inclusion was a negative LogP value of > 2.5. Two genes met the criterion in all three groups, *Tmem132d* and *Pkrcz*. (C) Exemplary scatter plots of candidate genes which were upregulated in PLX3397 treated mice. Genes were selected on the basis of the P-value, q-value and pathway enrichment i.e. more than one subtype of a gene (e.g. *Prkcz, Prkce*) or direct interaction (*Calm1, Camk2a*). (For interpretation of the references to colour in this figure legend, the reader is referred to the web version of this article.)

dominate over anti-apoptotic effects of M/M attenuation during the early phase of TBI. Our results are consistent with a recently proposed framework for future preclinical and clinical trials to tailor rather than block the immune response and to limit the acute pro-inflammatory response just to the level required for clearance of debris and danger signals (Simon et al., 2017).

Although CSF1R inhibition did not prevent early structural brain damage at 5 dpi, the early post-traumatic treatment reduced long-term brain tissue loss, improved hippocampal integrity, and attenuated thalamic neurodegeneration at 30 dpi. The protective effects on brain tissue loss and GCL structural integrity were evident both in male and female mice, whereas hippocampal atrophy, thalamic neurodegeneration, and the concomitant thalamic infiltration by $CD68^+$ M/M were significantly attenuated only in male mice. Sex-specific differences in clinical and experimental TBI have been described in several studies and also relate to M/M responses (Biegon, 2021; Morganti-Kossmann et al., 2019; Späni et al., 2018). Notably, sex-biased depletion efficacy upon PLX3397 treatment was reported despite equal drug concentrations in the brain (Berve et al., 2020; Easley-Neal et al., 2019). While we found little evidence for sex-specific PLX3397 efficacy after TBI at 5 dpi, PLX3997 decreased *Aif1* and *Csf1r* expression in male sham mice but not in female sham mice. However, minor differences of PLX3397 efficacy at 5 dpi do not readily explain the stronger benefit of PLX3397 treatment in male mice at 30 dpi. To clarify this question, further studies of the temporal and regional characteristics of sex-specific effects of CSF1R inhibitors with regard to depletion efficacy and neuroprotection are required including prolonged CSF1R inhibitor administration which has been shown to eliminate ~ 99 % of microglia in male mice (Elmore et al., 2014). Overall, our findings are consistent with recent studies demonstrating beneficial effects of microglia depletion via CSF1R inhibitors prior to experimental TBI or peri-operatively or continuously extending CSF1R inhibition into the subacute or chronic phases of TBI (Ritzel et al., 2021; Wang et al., 2020; Willis et al., 2020; Witcher et al., 2018).

Data from RNAseq and GSEA suggest that early CSF1R inhibition leads to long-term beneficial effects at the neuronal and synaptic levels, because up-regulated genes in the PLX3397 TBI group associated with the GO terms spine morphogenesis, synaptic vesicle exocytosis, and glutamate receptor signaling, among others (Supplementary information, Fig. S7). Among the key candidate genes are *Camk2a* and *Camk2b*, encoding for CaMKIIα and CaMKIIβ which form a dodecameric holoenzyme with pivotal functions in activity-dependent structural and synaptic plasticity (Hojjati et al., 2007; Incontro et al., 2018; Jourdain et al., 2003; Shibata et al., 2021). Members of the protein kinase C (PKC) family, including PKMζ encoded by *Pkrcz* (Hernandez et al., 2003), were also found among the upregulated genes and play critical functions in memory storage. Deficits in neuronal PKC signal cascades are one of the earliest abnormalities in the brains of Alzheimer's disease patients (Sun and Alkon, 2014). Other genes that were upregulated in the PLX3397 groups are also linked to synaptic plasticity, neurotransmission, learning and memory, and have been associated with neurological disorders as for example *LRCC4* encoding for NGL-1 (Um et al., 2018), or *Ptk2b* encoding for Pyk2 (Mastrolia et al., 2021; Salazar et al., 2019). Since TBI has been found to first reduce synapse density followed by synaptic recovery within few weeks (Norris and Scheff, 2009; Scheff et al., 2005), and to trigger molecular and cellular mechanisms that interfere with synapse maintenance and rebuilding (Jamjoom et al., 2021), our results suggest that early CSF1R inhibition improves long-term neuronal and synaptic maintenance and recovery. Interestingly, long-term elimination of microglia after diphtheria toxin-driven neuronal injury (Rice et al., 2015) or in the FPI model of TBI (Witcher et al., 2021) increased spine densities. Microglia elimination also prevented FPI-induced neuronal connectivity deficits and impairment of cognitive functions (Bray et al., 2022; Witcher et al., 2021) suggesting that repopulated microglia in our TBI model are rather silent or permissive in terms of synapse formation and modelling. However, it should be considered that enhanced synaptic re-organization could not only promote brain repair but also an imbalance between excitatory and inhibitory neurotransmission and thereby increase the risk of post-traumatic epilepsy (Hunt et al., 2013).

In this study, the vehicle TBI group expressed more genes encoding for ribosomal proteins than the PLX3397 TBI group suggesting high metabolic and proliferative cellular activity. We favor the possibility that these up-regulations are due to M/M. In support of this, single-cell RNAseq indicated that microglia resistant to CSF1R inhibition expressed an overabundance of mRNA encoding ribosomal proteins in the FPI model of TBI (Witcher et al., 2021). In addition, our results from GSEA revealed in vehicle vs PLX3397 TBI mice at 30 dpi more genes associated with oxidative phosphorylation, electron transfer activity, and oxidoreductase activity. This result suggests higher production of reactive oxygen, nitrogen species and oxidative stress which can alter neuronal excitability via modification of synaptic proteins, uptake and release of neurotransmitters and ion gradients (Ansari et al., 2008; Beckhauser et al., 2016; Love, 1999). The RNAseq results that point to increased oxidative metabolism in the vehicle group are supported by recent findings showing anti-oxidative stress effects of the CSF1R inhibitor PLX5622 in the chronic phase of TBI (Henry et al., 2020). Along this line, early administration of minocycline, which has potent anti-inflammatory and anti-oxidant properties, reduces long-term synapse loss after experimental TBI (Celorrio et al., 2022). Our results thus provide further evidence for a close association between M/M−mediated inflammation, oxidative stress, and synapse loss in TBI.

Neurodegenerative models also provide evidence that subsets of microglia, or microglia-deficient or silencing genes such as *Grn*, encoding for progranulin, contribute to synaptic pruning (Lui et al., 2016). Data from TBI models are rare, but experiments modeling other types of brain injury suggest that microglia and other immune cells are crucial for the formation and strengthening of new synaptic connections (Simon et al., 2017). In experimental stroke, prolonged contacts between microglia and synapses lead to the disappearance of synapses (Wake et al., 2009). Therefore, M/M may contribute to ongoing restructuring of synapses after TBI, perhaps preventing the production of certain types of synapses, and resulting in a net reduction (Jamjoom et al., 2021).

In conclusion, this study shows that early post-traumatic administration of the CSF1R inhibitor PLX3397 for 5 days attenuates long-term neurodegeneration. However, PLX3397 attenuated M/M only by 50 % and both beneficial and detrimental functions of M/M were affected during the early phase of TBI. Overall effects were not sex-specific but several indices of better long-term treatment response in males are provided that warrant further considerations.

Authors contributions

Y.W., I.W., J.S., S.L., D.A., M.K., K.R., R.G., I.T. performed experiments and data analysis. J.S., K.R., R.G., and M.S. conceived experiments and animal testing protocols, M.S. performed the study design, Y. W., I.T. and M.S. wrote the manuscript. All authors approved the final manuscript.

6. Availability of data and materials

All data are available upon reasonable request. RNAseq data have been deposited as GEO dataset with the provisional accession number

GSE196121. To review GEO accession GSE196121, go to: https://emea01.safelinks.protection.outlook.com/?url=https%3A%2F%2Fwww.ncbi.nlm.nih.gov%2Fgeo%2Fquery%2Facc.cgi%3Facc%3DGSE196121&data=04%7C01%7C%7C1326527926c14cc4db3008d9e8ac4e2e%7C84df9e7fe9f640afb435aaaaaaaaaaaa%7C1%7C0%7C637796649018766690%7CUnknown%7CTWFpbGZsb3d8eyJWIjoiMC4wLjAwMDAiLCJQIjoiV2luMzIiLCJBTiI6Ik1haWwiLCJXVCI6Mn0%3D%7C3000&sdata=jdcXeuKHZGsd6kVRfcwZqA4CBD%2FFv1eX9p61UAeOJXc%3D&reserved=0 Enter token: qlezyaqsrluhbyx into the box.

Declaration of Competing Interest

The authors declare that they have no known competing financial interests or personal relationships that could have appeared to influence the work reported in this paper.

Acknowledgements

This study was supported by the Deutsche Forschungsgemeinschaft to M.S. (SCHA 1261/4-3) and to I.T. (CRC1080 C02) and the Research Center for Immunotherapy (FZI) to M.S. Data shown in this manuscript are part of the doctoral thesis of Y.W. presented to the Johannes Gutenberg-University Mainz. Y.W. and S.L. are financially supported by the China Scholarship Council. We gratefully acknowledge the excellent technical assistance of Dana Pieter and Tobias Hirnet.

Appendix A. Supplementary data

Supplementary data to this article can be found online at https://doi.org/10.1016/j.bbi.2022.07.164.

References

Abdul-Muneer, P.M., Chandra, N., Haorah, J., 2015. Interactions of oxidative stress and neurovascular inflammation in the pathogenesis of traumatic brain injury. Mol. Neurobiol. 51, 966–979.
Akamatsu, Y., Hanafy, K.A., 2020. Cell Death and Recovery in Traumatic Brain Injury. Neurotherapeutics. 17, 446–456.
Alam, A., Thelin, E.P., Tajsic, T., Khan, D.Z., Khellaf, A., Patani, R., Helmy, A., 2020. Cellular infiltration in traumatic brain injury. J Neuroinflammation. 17, 328.
Ansari, M.A., Roberts, K.N., Scheff, S.W., 2008. Oxidative stress and modification of synaptic proteins in hippocampus after traumatic brain injury. Free Radic. Biol. Med. 45, 443–452.
Beckhauser, T.F., Francis-Oliveira, J., De Pasquale, R., 2016. Reactive Oxygen Species: Physiological and Physiopathological Effects on Synaptic Plasticity. J. Exp. Neurosci. 10, 23–48.
Bermpohl, D., You, Z., Lo, E.H., Kim, H.H., Whalen, M.J., 2007. TNF alpha and Fas mediate tissue damage and functional outcome after traumatic brain injury in mice. J. Cereb. Blood Flow Metab. 27, 1806–1818.
Berve, K., West, B.L., Martini, R., Groh, J., 2020. Sex- and region-biased depletion of microglia/macrophages attenuates CLN1 disease in mice. J. Neuroinflam. 17, 323.
Biegon, A., 2021. Considering Biological Sex in Traumatic Brain Injury. Front. Neurol. 12, 576366.
Bodnar, C.N., Watson, J.B., Higgins, E.K., Quan, N., Bachstetter, A.D., 2021. Inflammatory Regulation of CNS Barriers After Traumatic Brain Injury: A Tale Directed by Interleukin-1. Front. Immunol. 12, 688254.
Bolte, A.C., Lukens, J.R., 2021. Neuroimmune cleanup crews in brain injury. Trends Immunol. 42, 480–494.
Bourke, E., Cassetti, A., Villa, A., Fadlon, E., Colotta, F., Mantovani, A., 2003. IL-1β Scavenging by the Type II IL-1 Decoy Receptor in Human Neutrophils. 170:5999-6005.
Bray, C.E., Witcher, K.G., Adekunle-Adegbite, D., Ouvina, M., Witzel, M., Hans, E., Tapp, Z.M., Packer, J., Goodman, E., Zhao, F., Chunchai, T., O'Neil, S., Chattipakorn, S.C., Sheridan, J., Kokiko-Cochran, O.N., Askwith, C., Godbout, J.P., 2022. Chronic cortical inflammation, cognitive impairment and immune reactivity associated with diffuse brain injury are ameliorated by forced turnover of microglia. J. Neurosci.
Brockhaus, J., Möller, T., Kettenmann, H., 1996. Phagocytozing ameboid microglial cells studied in a mouse corpus callosum slice preparation. Glia. 16, 81–90.
Caplan, H.W., Cox, C.S., Bedi, S.S., 2017. Do microglia play a role in sex differences in TBI? J. Neurosci. Res. 95, 509–517.
Celorrio, M., Shumilov, K., Payne, C., Vadivelu, S., Friess, S.H., 2022. Acute minocycline administration reduces brain injury and improves long-term functional outcomes after delayed hypoxemia following traumatic brain injury. Acta Neuropathol. Commun. 10, 10.
Chao, C.C., Hu, S., Ehrlich, L., Peterson, P.K., 1995. Interleukin-1 and tumor necrosis factor-alpha synergistically mediate neurotoxicity: involvement of nitric oxide and of N-methyl-D-aspartate receptors. Brain Behav. Immun. 9, 355–365.
Clausen, F., Hånell, A., Björk, M., Hillered, L., Mir, A.K., Gram, H., Marklund, N., 2009. Neutralization of interleukin-1beta modifies the inflammatory response and improves histological and cognitive outcome following traumatic brain injury in mice. Eur. J. Neurosci. 30, 385–396.
De, I., Nikodemova, M., Steffen, M.D., Sokn, E., Maklakova, V.I., Watters, J.J., Collier, L. S., 2014. CSF1 overexpression has pleiotropic effects on microglia in vivo. Glia. 62, 1955–1967.
Delaney, C., Farrell, M., Doherty, C.P., Brennan, K., O'Keeffe, E., Greene, C., Byrne, K., Kelly, E., Birmingham, N., Hickey, P., Cronin, S., Savvides, S.N., Doyle, S.L., Campbell, M., 2021. Attenuated CSF-1R signalling drives cerebrovascular pathology. EMBO Mol. Med. 13, e12889–e.
Dewan, M.C., Rattani, A., Gupta, S., Baticulon, R.E., Hung, Y.C., Punchak, M., Agrawal, A., Adeleye, A.O., Shrime, M.G., Rubiano, A.M., Rosenfeld, J.V., Park, K.B., 2018. Estimating the global incidence of traumatic brain injury. J. Neurosurg. 1–18.
Donat, C.K., Gaber, K., Meixensberger, J., Brust, P., Pinborg, L.H., Hansen, H.H., Mikkelsen, J.D., 2016. Changes in Binding of [(123)I]CLINDE, a High-Affinity Translocator Protein 18 kDa (TSPO) Selective Radioligand in a Rat Model of Traumatic Brain Injury. Neuromol. Med. 18, 158–169.
Donat, C.K., Scott, G., Gentleman, S.M., Sastre, M., 2017. Microglial activation in traumatic brain injury. Front. Aging Neurosci. 9, 208.
Easley-Neal, C., Foreman, O., Sharma, N., Zarrin, A.A., Weimer, R.M., 2019. CSF1R Ligands IL-34 and CSF1 Are Differentially Required for Microglia Development and Maintenance in White and Gray Matter Brain Regions. Front. Immunol. 10, 2199.
Eden, E., Navon, R., Steinfeld, I., Lipson, D., Yakhini, Z., 2009. GOrilla: a tool for discovery and visualization of enriched GO terms in ranked gene lists. BMC Bioinf. 10, 48.
Elmore, M.R., Najafi, A.R., Koike, M.A., Dagher, N.N., Spangenberg, E.E., Rice, R.A., Kitazawa, M., Matusow, B., Nguyen, H., West, B.L., Green, K.N., 2014. Colony-stimulating factor 1 receptor signaling is necessary for microglia viability, unmasking a microglia progenitor cell in the adult brain. Neuron 82, 380–397.
Glushakov, A.O., Glushakova, O.Y., Korol, T.Y., Acosta, S.A., Borlongan, C.V., Valadka, A.B., Hayes, R.L., Glushakov, A.V., 2018. Chronic Upregulation of Cleaved-Caspase-3 Associated with Chronic Myelin Pathology and Microvascular Reorganization in the Thalamus after Traumatic Brain Injury in Rats. Int. J. Mol. Sci. 19, 3151.
Green, K.N., Crapser, J.D., Hohsfield, L.A., 2020. To Kill a Microglia: A Case for CSF1R Inhibitors. Trends Immunol. 41, 771–784.
Guadagno, J., Xu, X., Karajgikar, M., Brown, A., Cregan, S.P., 2013. Microglia-derived TNFα induces apoptosis in neural precursor cells via transcriptional activation of the Bcl-2 family member Puma. Cell Death Dis. 4, e538–e.
Han, J., Zhu, K., Zhang, X.M., Harris, R.A., 2019. Enforced microglial depletion and repopulation as a promising strategy for the treatment of neurological disorders. Glia. 67, 217–231.
Han, J., Fan, Y., Zhou, K., Blomgren, K., Harris, R.A., 2021. Uncovering sex differences of rodent microglia. J. Neuroinflam. 18, 74.
Hanlon, L.A., Raghupathi, R., Huh, J.W., 2019. Depletion of microglia immediately following traumatic brain injury in the pediatric rat: Implications for cellular and behavioral pathology. Exp. Neurol. 316, 39–51.
Haruwaka, K., Ikegami, A., Tachibana, Y., Ohno, N., Konishi, H., Hashimoto, A., Matsumoto, M., Kato, D., Ono, R., Kiyama, H., Moorhouse, A.J., Nabekura, J., Wake, H., 2019. Dual microglia effects on blood brain barrier permeability induced by systemic inflammation. Nat. Commun. 10, 5816.
Henry, R.J., Ritzel, R.M., Barrett, J.P., Doran, S.J., Jiao, Y., Leach, J.B., Szeto, G.L., Wu, J., Stoica, B.A., Faden, A.I., Loane, D.J., 2020. Microglial Depletion with CSF1R inhibitor during chronic phase of experimental traumatic brain injury reduces neurodegeneration and neurological deficits. J. Neurosci. 40, 2960–2974.
Hernandez, A.I., Blace, N., Crary, J.F., Serrano, P.A., Leitges, M., Libien, J.M., Weinstein, G., Tcherapanov, A., Sacktor, T.C., 2003. Protein kinase M zeta synthesis from a brain mRNA encoding an independent protein kinase C zeta catalytic domain. Implications for the molecular mechanism of memory. J. Biol. Chem. 278, 40305–40316.
Herzog, C., Pons Garcia, L., Keatinge, M., Greenald, D., Moritz, C., Peri, F., Herrgen, L., 2019. Rapid clearance of cellular debris by microglia limits secondary neuronal cell death after brain injury in vivo. Development. 146.
Hilla, A.M., Diekmann, H., Fischer, D., 2017. Microglia Are Irrelevant for Neuronal Degeneration and Axon Regeneration after Acute Injury. J. Neurosci. 37, 6113–6124.
Hojjati, M.R., van Woerden, G.M., Tyler, W.J., Giese, K.P., Silva, A.J., Pozzo-Miller, L., Elgersma, Y., 2007. Kinase activity is not required for alphaCaMKII-dependent presynaptic plasticity at CA3-CA1 synapses. Nat. Neurosci. 10, 1125–1127.
Hosomi, S., Kitamura, T., Sobue, T., Ogura, H., Shimazu, T., 2021. Sex and age differences in isolated traumatic brain injury: a retrospective observational study. BMC Neurol. 21, 261.
Hummel, R., Ulbrich, S., Appel, D., Li, S., Hirnet, T., Zander, S., Bobkiewicz, W., Gölz, C., Schäfer, M.K.E., 2020. Administration of all-trans retinoic acid after experimental traumatic brain injury is brain protective. Br. J. Pharmacol. 177, 5208–5223.
Hummel, R., Lang, M., Walderbach, S., Wang, Y., Tegeder, I., Gölz, C., Schäfer, M.K.E., 2021. Single intracerebroventricular progranulin injection adversely affects the blood-brain barrier in experimental traumatic brain injury. J. Neurochem. 158, 342–357.

Hunt, R.F., Boychuk, J.A., Smith, B.N., 2013. Neural circuit mechanisms of post-traumatic epilepsy. Front. Cell. Neurosci. 7, 89.
Incontro, S., J. Díaz-Alonso, J. Iafrati, M. Vieira, C.S. Asensio, V.S. Sohal, K.W. Roche, K. J. Bender, and R.A. Nicoll. 2018. The CaMKII/NMDA receptor complex controls hippocampal synaptic transmission by kinase-dependent and independent mechanisms. Nature communications. 9:2069-2069.
Jamjoom, A.A.B., Rhodes, J., Andrews, P.J.D., Grant, S.G.N., 2021. The synapse in traumatic brain injury. Brain. 144, 18–31.
Jassam, Y.N., Izzy, S., Whalen, M., McGavern, D.B., El Khoury, J., 2017. Neuroimmunology of Traumatic Brain Injury: Time for a Paradigm Shift. Neuron 95, 1246–1265.
Jolivel, V., Bicker, F., Binamé, F., Ploen, R., Keller, S., Gollan, R., Jurek, B., Birkenstock, J., Poisa-Beiro, L., Bruttger, J., Opitz, V., Thal, S.C., Waisman, A., Bäuerle, T., Schäfer, M.K., Zipp, F., Schmidt, M.H.H., 2015. Perivascular microglia promote blood vessel disintegration in the ischemic penumbra. Acta Neuropathol. 129, 279–295.
Jourdain, P., Fukunaga, K., Muller, D., 2003. Calcium/calmodulin-dependent protein kinase II contributes to activity-dependent filopodia growth and spine formation. J. Neurosci. 23, 10645–10649.
Karve, I.P., Taylor, J.M., Crack, P.J., 2016. The contribution of astrocytes and microglia to traumatic brain injury. Br. J. Pharmacol. 173, 692–702.
Lan, X., Han, X., Li, Q., Yang, Q.W., Wang, J., 2017. Modulators of microglial activation and polarization after intracerebral haemorrhage. Nat. Rev. Neurol. 13, 420–433.
Loane, D.J., Kumar, A., 2016. Microglia in the TBI brain: The good, the bad, and the dysregulated. Exp. Neurol. 275 (Pt 3), 316–327.
Love, S., 1999. Oxidative stress in brain ischemia. Brain Pathol. 9, 119–131.
Lu, K.T., Wang, Y.W., Yang, J.T., Yang, Y.L., Chen, H.I., 2005. Effect of interleukin-1 on traumatic brain injury-induced damage to hippocampal neurons. J. Neurotrauma 22, 885–895.
Lui, H., Zhang, J., Makinson, S.R., Cahill, M.K., Kelley, K.W., Huang, H.Y., Shang, Y., Oldham, M.C., Martens, L.H., Gao, F., Coppola, G., Sloan, S.A., Hsieh, C.L., Kim, C.C., Bigio, E.H., Weintraub, S., Mesulam, M.M., Rademakers, R., Mackenzie, I.R., Seeley, W.W., Karydas, A., Miller, B.L., Borroni, B., Ghidoni, R., Farese Jr., R.V., Paz, J.T., Barres, B.A., Huang, E.J., 2016. Progranulin Deficiency Promotes Circuit-Specific Synaptic Pruning by Microglia via Complement Activation. Cell 165, 921–935.
Mastrolia, V., Al Massadi, O., de Pins, B., Girault, J.A., 2021. Pyk2 in dorsal hippocampus plays a selective role in spatial memory and synaptic plasticity. Sci. Rep. 11, 16357.
McConeghy, K.W., Hatton, J., Hughes, L., Cook, A.M., 2012. A review of neuroprotection pharmacology and therapies in patients with acute traumatic brain injury. CNS Drugs. 26, 613–636.
Morganti-Kossmann, M.C., Semple, B.D., Hellewell, S.C., Bye, N., Ziebell, J.M., 2019. The complexity of neuroinflammation consequent to traumatic brain injury: from research evidence to potential treatments. Acta Neuropathol. 137, 731–755.
Neher, J.J., Emmrich, J.V., Fricker, M., Mander, P.K., Théry, C., Brown, G.C., 2013. Phagocytosis executes delayed neuronal death after focal brain ischemia. Proc Natl Acad Sci U S A. 110:E4098-4107.
Neumann, H., Kotter, M.R., Franklin, R.J., 2009. Debris clearance by microglia: an essential link between degeneration and regeneration. Brain. 132, 288–295.
Newell, E.A., Todd, B.P., Luo, Z., Evans, L.P., Ferguson, P.J., Bassuk, A.G., 2020. A Mouse Model for Juvenile, Lateral Fluid Percussion Brain Injury Reveals Sex-Dependent Differences in Neuroinflammation and Functional Recovery. J. Neurotrauma 37, 635–646.
Norris, C.M., Scheff, S.W., 2009. Recovery of afferent function and synaptic strength in hippocampal CA1 following traumatic brain injury. J. Neurotrauma 26, 2269–2278.
Ramlackhansingh, A.F., Brooks, D.J., Greenwood, R.J., Bose, S.K., Turkheimer, F.E., Kinnunen, K.M., Gentleman, S., Heckemann, R.A., Gunanayagam, K., Gelosa, G., Sharp, D.J., 2011. Inflammation after trauma: microglial activation and traumatic brain injury. Ann. Neurol. 70, 374–383.
Ransohoff, R.M., 2016. A polarizing question: do M1 and M2 microglia exist? Nat. Neurosci. 19, 987–991.
Rice, R.A., Spangenberg, E.E., Yamate-Morgan, H., Lee, R.J., Arora, R.P., Hernandez, M. X., Tenner, A.J., West, B.L., Green, K.N., 2015. Elimination of Microglia Improves Functional Outcomes Following Extensive Neuronal Loss in the Hippocampus. J. Neurosci. 35, 9977–9989.
Ritter, K., Jung, K., Dolderer, C., Appel, D., Oswald, C.C., Ritz, U., Schäfer, M.K.E., 2021. Early reciprocal effects in a murine model of traumatic brain injury and femoral fracture. Mediators Inflamm. 2021, 8835730.
Ritzel, R.M., He, J., Li, Y., Cao, T., Khan, N., Shim, B., Sabirzhanov, B., Aubrecht, T., Stoica, B.A., Faden, A.I., Wu, L.J., Wu, J., 2021. Proton extrusion during oxidative burst in microglia exacerbates pathological acidosis following traumatic brain injury. Glia. 69, 746–764.
Salazar, S.V., Cox, T.O., Lee, S., Brody, A.H., Chyung, A.S., Haas, L.T., Strittmatter, S.M., 2019. Alzheimer's Disease Risk Factor Pyk2 Mediates Amyloid-β-Induced Synaptic Dysfunction and Loss. J. Neurosci. 39, 758–772.
Schäfer, M.K., Pfeiffer, A., Jaeckel, M., Pouya, A., Dolga, A.M., Methner, A., 2014. Regulators of mitochondrial Ca(2+) homeostasis in cerebral ischemia. Cell Tissue Res. 357, 395–405.
Schäfer, M.K.E., Tegeder, I., 2018. NG2/CSPG4 and progranulin in the posttraumatic glial scar. Matrix Biol. 68–69, 571–588.
Scheff, S.W., Price, D.A., Hicks, R.R., Baldwin, S.A., Robinson, S., Brackney, C., 2005. Synaptogenesis in the hippocampal CA1 field following traumatic brain injury. J. Neurotrauma 22, 719–732.
Shibata, A.C.E., Ueda, H.H., Eto, K., Onda, M., Sato, A., Ohba, T., Nabekura, J., Murakoshi, H., 2021. Photoactivatable CaMKII induces synaptic plasticity in single synapses. Nat. Commun. 12, 751.
Simon, D.W., McGeachy, M.J., Bayır, H., Clark, R.S., Loane, D.J., Kochanek, P.M., 2017. The far-reaching scope of neuroinflammation after traumatic brain injury. Nat. Rev. Neurol. 13, 171–191.
Späni, C.B., Braun, D.J., Van Eldik, L.J., 2018. Sex-related responses after traumatic brain injury: Considerations for preclinical modeling. Front. Neuroendocrinol.
Subramanian, A., Tamayo, P., Mootha, V.K., Mukherjee, S., Ebert, B.L., Gillette, M.A., Paulovich, A., Pomeroy, S.L., Golub, T.R., Lander, E.S., Mesirov, J.P., 2005. Gene set enrichment analysis: a knowledge-based approach for interpreting genome-wide expression profiles. PNAS 102, 15545–15550.
Sun, M.K., Alkon, D.L., 2014. The "memory kinases": roles of PKC isoforms in signal processing and memory formation. Prog. Mol. Biol. Transl. Sci. 122, 31–59.
Thal, S.C., Wyschkon, S., Pieter, D., Engelhard, K., Werner, C., 2008. Selection of endogenous control genes for normalization of gene expression analysis after experimental brain trauma in mice. J. Neurotrauma 25, 785–794.
Thornton, P., Pinteaux, E., Gibson, R.M., Allan, S.M., Rothwell, N.J., 2006. Interleukin-1-induced neurotoxicity is mediated by glia and requires caspase activation and free radical release. J. Neurochem. 98, 258–266.
Um, S.M., Ha, S., Lee, H., Kim, J., Kim, K., Shin, W., Cho, Y.S., Roh, J.D., Kang, J., Yoo, T., Noh, Y.W., Choi, Y., Bae, Y.C., Kim, E., 2018. NGL-2 Deletion Leads to Autistic-like Behaviors Responsive to NMDAR Modulation. Cell Rep. 23, 3839–3851.
Villapol, S., Yaszemski, A.K., Logan, T.T., Sánchez-Lemus, E., Saavedra, J.M., Symes, A. J., 2012. Candesartan, an Angiotensin II AT1-Receptor Blocker and PPAR-γ Agonist, Reduces Lesion Volume and Improves Motor and Memory Function After Traumatic Brain Injury in Mice. Neuropsychopharmacology. 37, 2817–2829.
Villapol, S., Loane, D.J., Burns, M.P., 2017. Sexual dimorphism in the inflammatory response to traumatic brain injury. Glia. 65, 1423–1438.
Waisman, A., Ginhoux, F., Greter, M., Bruttger, J., 2015. Homeostasis of Microglia in the Adult Brain: Review of Novel Microglia Depletion Systems. Trends Immunol. 36, 625–636.
Wake, H., Moorhouse, A.J., Jinno, S., Kohsaka, S., Nabekura, J., 2009. Resting microglia directly monitor the functional state of synapses in vivo and determine the fate of ischemic terminals. J. Neurosci. 29, 3974–3980.
Wang, C.F., Zhao, C.C., Liu, W.L., Huang, X.J., Deng, Y.F., Jiang, J.Y., Li, W.P., 2020. Depletion of Microglia Attenuates Dendritic Spine Loss and Neuronal Apoptosis in the Acute Stage of Moderate Traumatic Brain Injury in Mice. J. Neurotrauma 37, 43–54.
Waterston, R.H., Lindblad-Toh, K., Birney, E., Rogers, J., Abril, J.F., Agarwal, P., Agarwala, R., Ainscough, R., Alexandersson, M., An, P., Antonarakis, S.E., Attwood, J., Baertsch, R., Bailey, J., Barlow, K., Beck, S., Berry, E., Birren, B., Bloom, T., Bork, P., Botcherby, M., Bray, N., Brent, M.R., Brown, D.G., Brown, S.D., Bult, C., Burton, J., Butler, J., Campbell, R.D., Carninci, P., Cawley, S., Chiaromonte, F., Chinwalla, A.T., Church, D.M., Clamp, M., Clee, C., Collins, F.S., Cook, L.L., Copley, R.R., Coulson, A., Couronne, O., Cuff, J., Curwen, V., Cutts, T., Daly, M., David, R., Davies, J., Delehaunty, K.D., Deri, J., Dermitzakis, E.T., Dewey, C., Dickens, N.J., Diekhans, M., Dodge, S., Dubchak, I., Dunn, D.M., Eddy, S. R., Elnitski, L., Emes, R.D., Eswara, P., Eyras, E., Felsenfeld, A., Fewell, G.A., Flicek, P., Foley, K., Frankel, W.N., Fulton, L.A., Fulton, R.S., Furey, T.S., Gage, D., Gibbs, R.A., Glusman, G., Gnerre, S., Goldman, N., Goodstadt, L., Grafham, D., Graves, T.A., Green, E.D., Gregory, S., Guigó, R., Guyer, M., Hardison, R.C., Haussler, D., Hayashizaki, Y., Hillier, L.W., Hinrichs, A., Hlavina, W., Holzer, T., Hsu, F., Hua, A., Hubbard, T., Hunt, A., Jackson, I., Jaffe, D.B., Johnson, L.S., Jones, M., Jones, T.A., Joy, A., Kamal, M., Karlsson, E.K., et al., 2002. Initial sequencing and comparative analysis of the mouse genome. Nature 420, 520–562.
Wennersten, A., Holmin, S., Mathiesen, T., 2003. Characterization of Bax and Bcl-2 in apoptosis after experimental traumatic brain injury in the rat. Acta Neuropathol. 105, 281–288.
Werner, C., Engelhard, K., 2007. Pathophysiology of traumatic brain injury. Br. J. Anaesth. 99, 4–9.
Willis, E.F., MacDonald, K.P.A., Nguyen, Q.H., Garrido, A.L., Gillespie, E.R., Harley, S.B. R., Bartlett, P.F., Schroder, W.A., Yates, A.G., Anthony, D.C., Rose-John, S., Ruitenberg, M.J., Vukovic, J., 2020. Repopulating Microglia Promote Brain Repair in an IL-6-Dependent Manner. Cell 180, 833–846.e816.
Witcher, K.G., Bray, C.E., Dziabis, J.E., McKim, D.B., Benner, B.N., Rowe, R.K., Kokiko-Cochran, O.N., Popovich, P.G., Lifshitz, J., Eiferman, D.S., Godbout, J.P., 2018. Traumatic brain injury-induced neuronal damage in the somatosensory cortex causes formation of rod-shaped microglia that promote astrogliosis and persistent neuroinflammation. Glia. 66, 2719–2736.
Witcher, K.G., Bray, C.E., Chunchai, T., Zhao, F., O'Neil, S.M., Gordillo, A.J., Campbell, W.A., McKim, D.B., Liu, X., Dziabis, J.E., Quan, N., Eiferman, D.S., Fischer, A.J., Kokiko-Cochran, O.N., Askwith, C., Godbout, J.P., 2021. Traumatic Brain Injury Causes Chronic Cortical Inflammation and Neuronal Dysfunction Mediated by Microglia. J. Neurosci. 41, 1597–1616.
Yakovlev, A.G., Knoblach, S.M., Fan, L., Fox, G.B., Goodnight, R., Faden, A.I., 1997. Activation of CPP32-like caspases contributes to neuronal apoptosis and neurological dysfunction after traumatic brain injury. J. Neurosci. 17, 7415–7424.
Ye, L., Huang, Y., Zhao, L., Li, Y., Sun, L., Zhou, Y., Qian, G., Zheng, J.C., 2013. IL-1β and TNF-α induce neurotoxicity through glutamate production: a potential role for neuronal glutaminase. J. Neurochem. 125, 897–908.